Ore Geology Reviews 69 (2015) 140–156

Contents lists available at ScienceDirect

Ore Geology Reviews

journal homepage: www.elsevier.com/locate/oregeorev

Migration paths and precipitation mechanisms of ore-forming fluids at the Shuiyindong Carlin-type gold deposit, Guizhou, China

Qin-Ping Tan [a,b], Yong Xia [a,*], Zhuo-Jun Xie [a,b], Jun Yan [a,b]

[a] State Key Laboratory of Ore Deposit Geochemistry, Institute of Geochemistry, Chinese Academy of Sciences, Guiyang 550002, China
[b] University of Chinese Academy of Sciences, Beijing 100049, China

ARTICLE INFO

Article history:
Received 25 February 2014
Received in revised form 16 January 2015
Accepted 3 February 2015
Available online 7 February 2015

Keywords:
Carlin-type gold deposit
Shuiyindong deposit
Southwestern Guizhou
Ore-forming fluid
Migration path
Precipitation mechanism

ABSTRACT

Shuiyindong is one of the largest and highest grade stratabound Carlin-type gold deposits in China. This paper reports on the results of petrographic studies, electron microprobe analyses (EMPA) of arsenian pyrite, and the mass transfer during mineralization and alteration, and it presents the deposit-scale distributions of Au, As, Sb, Hg, Tl, and trace elements in a representative cross section across the Shuiyindong Carlin-type gold deposit, Guizhou Province. The main objectives were to identify the precipitation mechanisms of minerals, or elements from fluids, and the migration paths of ore-forming fluids.

Petrographic and EMPA studies indicate that gold in the primary ores is mainly hosted by arsenian pyrite. Mass transfer associated with alteration and mineralization shows that Au, As, Sb, Hg, Tl, and S were significantly added to all mineralized rocks, Fe_2O_3 and SiO_2 were immobile in the main orebodies that are hosted in bioclastic limestone, and CaO, Na_2O, Sr, and Li were removed from country rocks. The relations between Fe and S indicate that the sedimentary rocks at the Shuiyindong deposit contain more iron than is needed to combine with all of their contained sulfur to form pyrite. This suggests that sulfidation and decarbonation were the principal mechanism of gold precipitation at the Shuiyindong deposit. Hg, Sb, and As commonly formed sulfide minerals, such as stibnite, realgar, and orpiment, in late-stage quartz–calcite veins, or absorbed by organic matter in argillite. Fluid cooling presumably led to depositions of stibnite, realgar, and orpiment in late-stage quartz–calcite veins. Organic matter likely served as a reductant in argillite for the ore fluids, causing the precipitation of As, Sb, Hg, and S, as well as Au.

Deposit-scale distributions of gold and other relevant elements reflect the passage of fluids through the rocks. Rock strata and structures allowed the ore-forming fluids to migrate horizontally along the unconformity surface of the Middle–Upper Permian, converge on the high position of an anticline, and then ascend into the overlying strata along the anticlinal axis. The distributions of the major and trace elements show that elements that accompanied the ore-forming fluids include Au, As, Sb, Hg, Tl, and S, and that Na_2O and Li were exhausted in the Longtan Formation at the anticlinal core during gold mineralization. The enrichment of Co, Cr, and Ni in the Longtan Formation at the anticlinal core might be associated with deformation that formed the anticline, or with gold mineralization. Different host rocks were preferentially mineralized by different elements. The bioclastic limestone is commonly enriched in Au, whereas the argillite is preferentially enriched in As, Hg, Sb, and Tl. The zonation of ore-forming elements in the deposit appears to be Sb–Tl–As–Hg–Au–Hg–As (from bottom to top). Enrichment of Au, As, Sb, Hg, and Tl provides useful guidance for the exploration for Carlin-type gold deposits in Guizhou. Anomalies of As and Hg in soil or stream sediment might be an important clue and these elements can be used as indicator elements. Ore-forming fluids migrated along the unconformity surface of the Middle–Upper Permian and the anticlinal axis, so these are favorable sites for exploration for Carlin-type gold deposits in Guizhou.

1. Introduction

Carlin-type gold deposits are known mainly in Nevada, in the United States (Radtke et al., 1980; Arehart, 1996), and in southwest China (Ashley et al., 1991; Li and Peters, 1999). Both regions have many features in common regarding certain aspects such as tectonic setting, ore and gangue mineral assemblages, wall rock alteration, and mineralization (Cline and Hofstra, 2000; Hu et al., 2002; Yigit and Hofstra, 2003; Peters et al., 2007; Cline et al., 2013). Currently, Carlin-type deposits are the most important sources of gold in the United States (Muntean et al., 2011; Lubben et al., 2012), but they account for only a small proportion of gold production in China (Xia, 2005; Su et al., 2012).

The Nevada Carlin-type gold deposits have been the subject of a large number of studies in several fields, such as structural ore-controls, isotope geochemistry, fluid-inclusion geochemistry, and gold-depositing

* Corresponding author.
E-mail addresses: 565310821@qq.com (Q.-P. Tan), xiayong@vip.gyig.ac.cn (Y. Xia).

http://dx.doi.org/10.1016/j.oregeorev.2015.02.006
0169-1368/

processes (Arehart et al., 1993; Stenger et al., 1998; Simon et al., 1999b; Peters, 2004; Kesler et al., 2005; Emsbo et al., 2006; Muntean et al., 2007; Barker et al., 2009; Lubben et al., 2012). Isocon plots (Grant, 1986) have been used to study gains and losses during mineralization and alteration and to identify the processes that deposited gold in Carlin-type deposits, Nevada (Radtke et al., 1972; Kuehn and Rose, 1992; Hofstra, 1994; Hofstra and Cline, 2000; Cail and Cline, 2001; Kesler et al., 2003; Yigit and Hofstra, 2003). Element fluxes during mineralization and alteration show that sulfidation and decarbonation are the mechanisms of gold precipitation (Bakken and Einaudi, 1986; Cail and Cline, 2001; Kesler et al., 2003; Yigit and Hofstra, 2003). The relation between gold, iron, and sulfide sulfur values also suggests that sulfidation is an important factor controlling the formation of Carlin-type gold deposits, Nevada (Stenger et al., 1998; Kesler et al., 2003; Ye et al., 2003).

Many studies in Nevada Carlin-type deposits have investigated the spatial distributions of gold and related elements (Stenger et al., 1998; Heitt et al., 2003; Theodore et al., 2003; Arehart and Donelick, 2006; de Almeida et al., 2010) and have determined the pathways of the ore-forming fluids (Longo et al., 2009; Muntean et al., 2010; Vaughan et al., 2010; Barker et al., 2013; Hickey et al., 2014a, 2014b). Stable isotopes of oxygen and carbon and thermal halos were used to trace fluid pathways at Turquoise Ridge, Banshee, Screamer, Pipeline, and Betze–Post deposits in Nevada (Muntean et al., 2010; Vaughan et al., 2010; Barker et al., 2013; Hickey et al., 2014a, 2014b).

Carlin-type gold deposits in Guizhou, China have also been the subject of many studies (Ashley et al., 1991; Hofstra et al., 2005; Peters et al., 2007; Su et al., 2009b; Zhang et al., 2010; Chen et al., 2011, 2014, 2015; Wang et al., 2013). However, the migration pathways of the ore-forming fluids, and the mechanisms of gold precipitation at the Shuiyindong gold deposit remain unclear. Recent studies of the Shuiyindong deposit have concluded that the combination of the effects of fluid reduction and sulfidation of wall-rock iron by H_2S-rich ore fluids was the most important mechanism of gold deposition (Su et al., 2009a, 2012). Basin paleotopographic highs, syndepositional faulting, and an unconformity-related burial sequence might have controlled the migration pathways of fluids and thus, controlled the distribution of the Carlin-type gold deposits in Guizhou (Liu et al., 2002).

Previous petrographic and electron microprobe analysis (EMPA) studies of the Shuiyindong gold deposit have generally focused on the main orebodies (Zhang et al., 2008; Su et al., 2012), and have documented that the gold in the primary ores is hosted primarily by arsenian pyrite and, in lesser amounts, by arsenopyrite (Liu, 2003; Fu et al., 2004; Su et al., 2008). The emphasis of the current study is on the examination of the orebodies and country rocks, documenting changes in mineral association during mineralization and alteration. Isocon diagrams have been used in this study to calculate gains and losses of major and trace elements during mineralization and alteration, and to identify the processes that deposited gold. Deposit-scale distributions of gold and other elements can reflect the passage of hydrothermal fluids through rocks. Therefore, in this study, a profile across the Shuiyindong gold deposit was established as the subject of research. A large number of whole-rock samples was collected and analyzed for Au, As, Hg, and other trace elements, and the spatial distributions of the elements along the profile were determined. The major aim of this paper is to determine the precipitation mechanisms of minerals, or elements from fluids, and the migration paths of ore-forming fluids, which provide an important basis for target generation for Carlin-type gold deposits in Guizhou.

2. Regional geology

The southwestern Guizhou Province, which borders Yunnan Province and the Guangxi Autonomous Region (Fig. 1), contains many Carlin-type gold deposits (Zhang et al., 2003; Su et al., 2009a; Chen et al., 2011). The southwestern Guizhou Province is located at the juncture of the southwestern margin of the Yangtze craton and the westward extension of the Youjiang fold belt of the South China fold system (Hu et al., 2002; Gu et al., 2007; Peters et al., 2007).

The regionally exposed bedrock is predominantly Devonian to Triassic in age, and the Triassic rocks are most common, followed by Permian rocks (Fig. 1). Carboniferous and Devonian rocks are exposed in the cores of some anticlines. Regional tectonic activity began in the Yanshanian Period, during which complex structural deformation events occurred. The deformation formed narrow anticlines, and gentle and wide synclines. Regional magmatic rocks are mainly Emeishan flood basalt at the top of the Middle to the Upper Permian unconformity, and alkaline ultramafic rocks that intruded Permian to Triassic units (Fig. 1). Geochronological studies have shown that the alkaline ultramafic rocks (120–85 Ma; Su, 2002; Liu et al., 2010) might have a genetic relation with the Carlin-type gold deposits in Guizhou (Xia, 2005).

The orebodies of the Carlin-type gold deposits in Guizhou are hosted primarily in Late Permian to Triassic limestone of variable impurity and calcareous clastic rocks. Typically, they are controlled by short-axis anticlines (domes) and associated fracture zones (e.g., the Shuiyindong gold deposit; Su et al., 2012), high-angle faults (e.g., the Lannigou gold deposit; Chen et al., 2011), and paleokarst planes or unconformity surfaces (e.g., Getang gold deposit; Zhang et al., 2003).

3. Geology of the Shuiyindong deposit

The Shuiyindong gold deposit lies approximately 20 km northwest of the town of Zhenfeng in southwestern Guizhou, China, and the deposit is located on the eastern limb of the Huijiabao anticline, which hosts a cluster of gold deposits (Fig. 1). Recent exploration and underground mining at Shuiyindong have revealed gold reserves of 263 tons with an average gold grade of 5 g/t. Features of the major rock types and structures of the Shuiyindong gold deposit are shown in the surface geological map and representative cross section (Figs. 2, 3), and a short summary of their characteristics is provided below.

Sedimentary rocks in the mining area are dominated by the Middle and Upper Permian and Lower Triassic strata (Fig. 2). The Middle Permian Maokou Formation is a massive bioclastic limestone conformably overlain by the Upper Permian Longtan, Changxing, and Dalong Formations, and the Lower Triassic Yelang and Yongningzhen Formations. The Longtan Formation is about 300 m thick in the Shuiyindong district, and it has been divided into three stratigraphic units (Liu, 2001). The first unit consists of argillite. The second unit consists of silty argillite intercalated with bioclastic limestone and coal seams. The third unit includes calcareous siltstone, sandstone, and argillite and bioclastic limestone. Gold mineralization is preferentially disseminated in bioclastic limestone and calcareous siltstone of the first and the second units of the Longtan Formation (Figs. 3, 4A). The unconformity surface of the Middle to Upper Permian contains strongly silicified brecciated limestone–argillite at the Shuiyindong gold deposit (Fig. 4B; Xia, 2005; Liu et al., 2009), and lower grade orebodies are hosted at the unconformity surface.

The rocks of the mining area have been deformed into the nearly E–W-trending Huijiabao anticline (Fig. 2). The limbs of the anticline are cut by reverse faults F101 and F105, which strike E–W and dip steeply to the north and south, respectively. A series of nearly N-trending normal faults cuts the reverse faults and commonly control mercury–thallium deposits, such as in the Lanmuchang mining area (Su et al., 2012).

Gold mineralization at the Shuiyindong deposit is closely associated with decarbonation, silicification, sulfidation, and dolomitization (Hu et al., 2002; Peters et al., 2007; Su et al., 2012), similar to the situation in Nevada, USA (Hofstra and Cline, 2000; Cline et al., 2005). Decarbonation of limestone is evident from small relict inclusions of calcite and dolomite in jasperoidal quartz (Hofstra and Cline, 2000; de Almeida et al., 2010). Decarbonation leads to a significant volume loss in some orebodies, and calcite and dolomite commonly fill the fractures in the

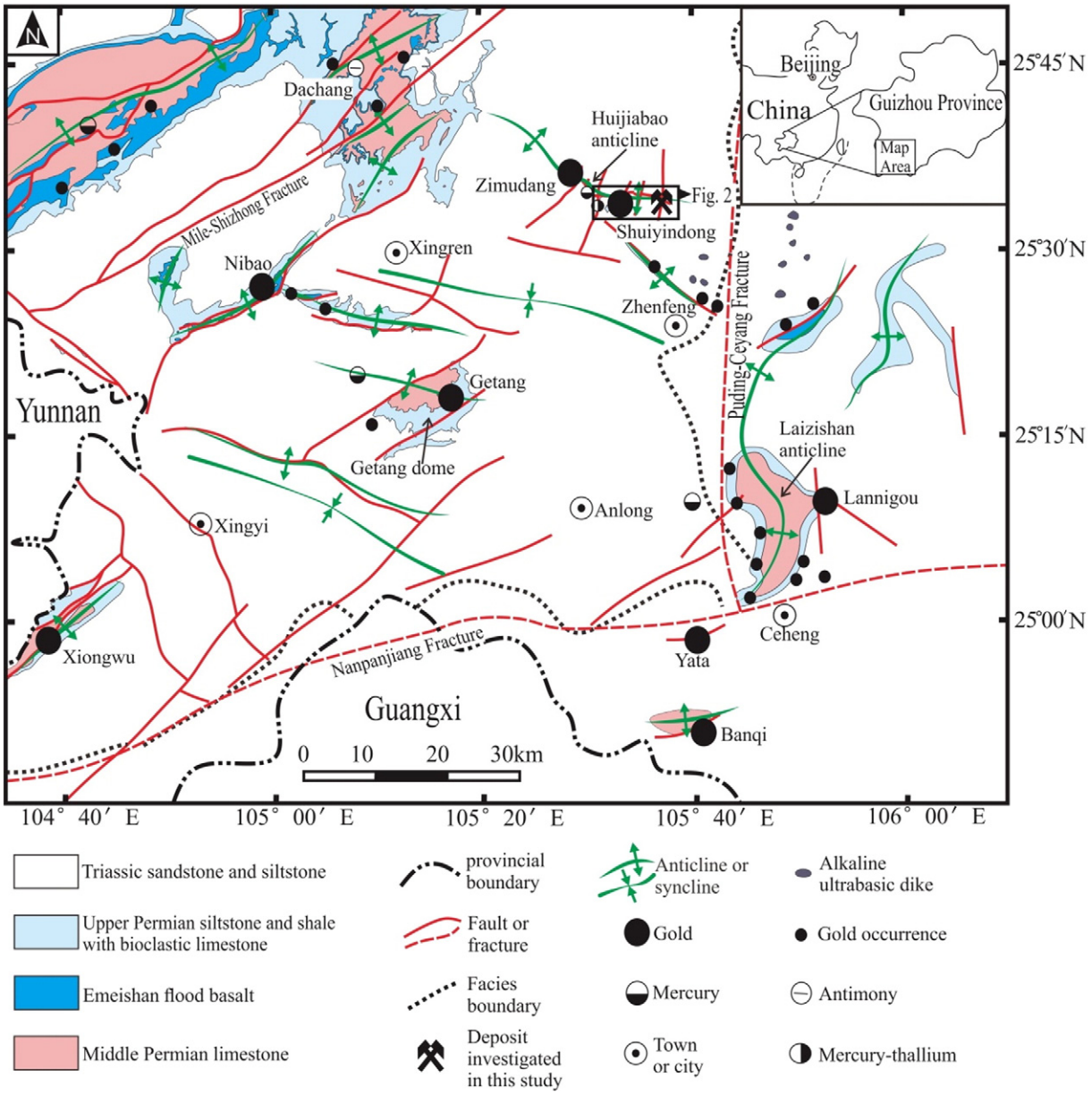

Fig. 1. Regional geological sketch map of southwestern Guizhou (modified after Su et al., 2009a; Zhang et al., 2003) showing the distribution of major Carlin-type gold, antimony, and mercury deposits. The deposits are typically controlled by short-axis anticlines (domes) and associated fracture zones, high-angle faults, and paleokarst planes or unconformity surfaces.

peripheral zones of decarbonated rocks (Fig. 4D). Sulfide minerals in the deposit consist mainly of arsenian pyrite, arsenopyrite, marcasite, and small amounts of orpiment, realgar, and stibnite. Small amounts of gold-bearing arsenian pyrite and arsenopyrite are enclosed within Fe-bearing dolomite, whereas large amounts of gold-bearing arsenian pyrite and arsenopyrite are concentrated along jasperoidal quartz grain boundaries or enclosed within jasperoidal quartz grains where the dolomite has been partially dissolved (Fig. 5D). Arsenian pyrite formed earlier than arsenopyrite in the paragenetic sequence because arsenopyrite occurs as overgrowths on arsenian pyrite (Fig. 4H). Arsenian pyrite also forms rims on framboidal pyrite cores of diagenetic origin (Fig. 4I). Gangue minerals consist of quartz, dolomite, calcite, and clay minerals (e.g., kaolinite). Stibnite, realgar, pyrite, and orpiment commonly occur at the unconformity surface, the microcracks of the Longtan Formation and the reverse faults with late-stage quartz–calcite veins (Fig. 4C, D, E, G). Bitumen in the gold deposit is commonly present in orebodies, particularly close to high grade ores (Fig. 4F).

4. Sampling and analytical methods

For this study, a representative N–S cross section across the Shuiyindong gold deposit was selected. This cross section was chosen because of its relatively simple ore-controlling structures and because it contains almost every sedimentary rock unit within the mining area. In total, 350 samples were collected from 8 drill holes, the positions of which are shown in Fig. 3. The whole-rock samples were cleaned with deionized water, crushed, and then powdered in an agate mill. All samples were analyzed for contents of Au, As, Hg, and other trace elements. Numbered samples in Fig. 3 were also analyzed for major elements. The samples with a number shown within a rectangular frame in Fig. 3 were chosen for backscattered electron (BSE) imaging and EMPA of arsenian pyrite. All data were obtained using accepted analytical methods, and the data are listed in Appendix A.

EMPA and the analyses of the major and trace elements were performed at the State Key Laboratory of Ore Deposit Geochemistry, Institute of Geochemistry, Chinese Academy of Sciences. Gold, total sulfur,

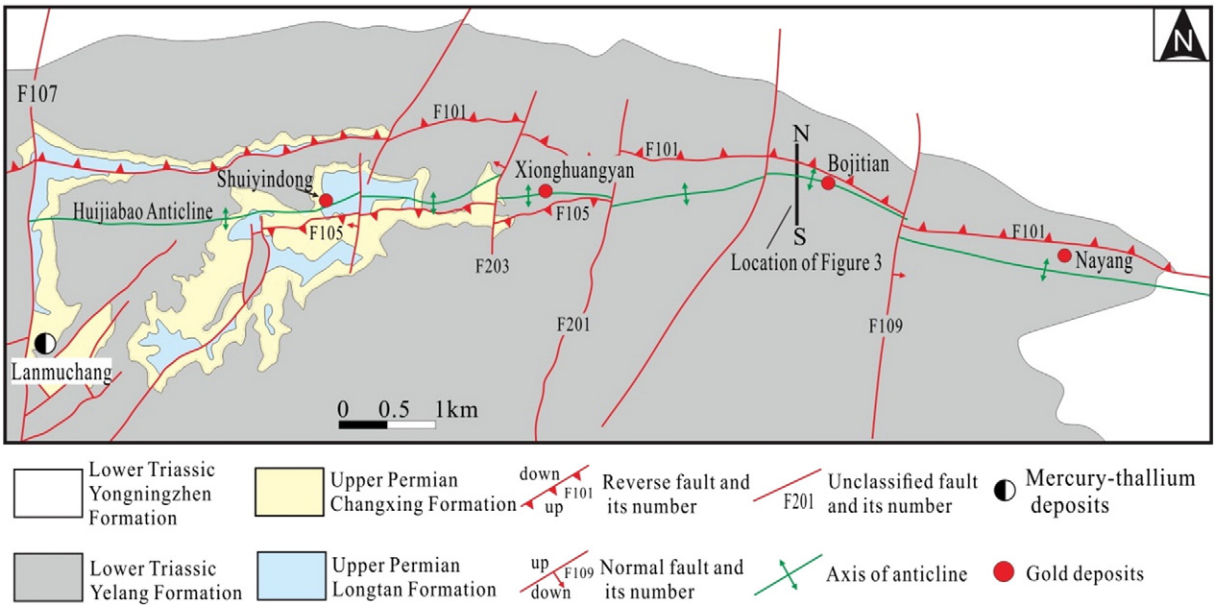

Fig. 2. Geological plan map of the Shuiyindong mining area showing rock formations and structures. The location of the mining area is shown in Fig. 1.

arsenic, and mercury were analyzed by ALS-Chemex (Guangzhou) commercial laboratories. The analytical methods are described below.

Backscattered electron (BSE) imaging and chemical analyses of arsenian pyrite were performed on EPMA-1600 (Shimadzu, Japan) electron probe microanalyzer equipped with five X-ray wavelength dispersive spectrometers (WDS). An EDAX energy dispersive spectrometer (EDS) on the EMPA was used to identify minerals. Iron, S, As, Cu, Sb, Cr, Hg and Au were detected in arsenian pyrite using a 25 keV accelerating voltage, 10–40 nA beam current, and a 10 s-counting time. With our operating conditions, the detection limit of Au in arsenian pyrite is about 400 ppm. Standards used were natural marcasite for Fe and S, GaAs (Alfa, Aesar, USA) for As, cuprite for Cu, cinnabar for Hg, crocoite for Cr and native gold for Au.

Major elements were analyzed with a PANalytical Axios-advance (Axios PW4400) X-ray fluorescence spectrometer (XRF). Fused glass discs were used and the analytical precision as determined on the Chinese National standard GSR-3 was better than 5%. Loss on ignition (LOI) was obtained using 1 g of powder, heated to 1100 °C for 1 h.

Total sulfur was analyzed using a Leco sulfur analyzer. The sample is heated to approximately 1350 °C in an induction furnace while passing a stream of oxygen through the sample. Sulfur dioxide released from the sample is measured by an IR detection system and the total sulfur result is provided.

The trace elements were analyzed using a Perkin-Elmer Sciex ELAN 6000 ICP-MS. The powdered samples (50 mg) were dissolved in high-pressure Teflon bombs using a HF + HNO_3 mixture for 48 h at 190 °C. Rh was used as an internal standard to monitor signal drift during counting. Analyses of international standards OU-6 and GBPG-1 are in agreement with recommended values, and analytical precision was generally better than 5% for all elements. This method provided data for Sb, Tl, Li, Be, Sc, V, Cr, Co, Ni, Cu, Zn, Ga, Ge, Rb, Sr, Y, Zr, Nb, Mo, Cs, Ba, Hf, Ta, W, Pb, Th, U, and 14 of the rare earth elements.

Gold (fire assay): samples were fused with a mixture of lead oxide, sodium carbonate, borax, silica and other reagents as required, inquarted with 6 mg of gold-free silver and then cupelled to yield a precious metal bead. The bead was digested in 0.5 ml dilute nitric acid in the microwave oven, 0.5 ml concentrated hydrochloric acid was then added and the bead was further digested in the microwave at a lower power setting. The digested solution was cooled, diluted to a total volume of 4 ml with de-mineralized water, and then analyzed by atomic absorption spectroscopy against matrix-matched standards.

Arsenic: samples were digested with perchloric, nitric, hydrofluoric and hydrochloric acids. The residue was topped up with dilute hydrochloric acid and the resulting solution was analyzed by inductively coupled plasma-atomic emission spectrometry. Results were corrected for spectral inter-element interferences.

Mercury: samples were digested with aqua regia in a graphite heating block. After cooling, the resulting solution was diluted with deionized water, mixed and analyzed by inductively coupled plasma-atomic emission spectrometry. The analytical results were corrected for inter-element spectral interferences.

5. Results

5.1. Petrographic studies

Samples 23940-9 and 23902-32 represent the country rocks and orebodies within the same bioclastic limestone layer of the Changxing Formation (Fig. 5A, B), and the location of the two samples is shown in Fig. 3. Petrographic studies indicate that orebodies and country rocks of the Changxing Formation both developed microcracks and filled with minerals, such as quartz, arsenian pyrite, and arsenopyrite, as well as organic matter. The organic matter dispersed in the orebodies and country rocks occurs with quartz, and it is typically concentrated along the walls of pores and fractures. Large amounts of gold-bearing arsenian pyrite (Au: 410–840 ppm; Table 1) and arsenopyrite are concentrated in the orebodies (Fig. 5B), whereas only small amounts of gold-poor arsenian pyrite (Table 1) occur in country rocks (Fig. 5A).

Samples 23940-43 and 23902-97 represent the country rocks and orebodies within the same bioclastic limestone layer of the Longtan Formation (Fig. 5C, D), and the location of the two samples are shown in Fig. 3. Petrographic studies indicate that minerals in the country rocks (Fig. 5C) include few globular gold-poor arsenian pyrite (Table 1), imporous ferroan dolomite, and quartz. A large amount of gold-bearing arsenian pyrite (Au: 510–1320 ppm; Table 1) is concentrated along the quartz boundaries, or included in the quartz grains in the orebodies (Fig. 5D). Organic matter, apatite and sphalerite also occurred in the orebodies. Porous ferroan dolomite does not contain gold-bearing arsenian pyrite in the orebodies; calcite tends to occur next to the ferroan dolomite.

Samples 23940-57 and 23916-58 represent the country rock and mineralized rock within the same argillite layer of the Longtan Formation

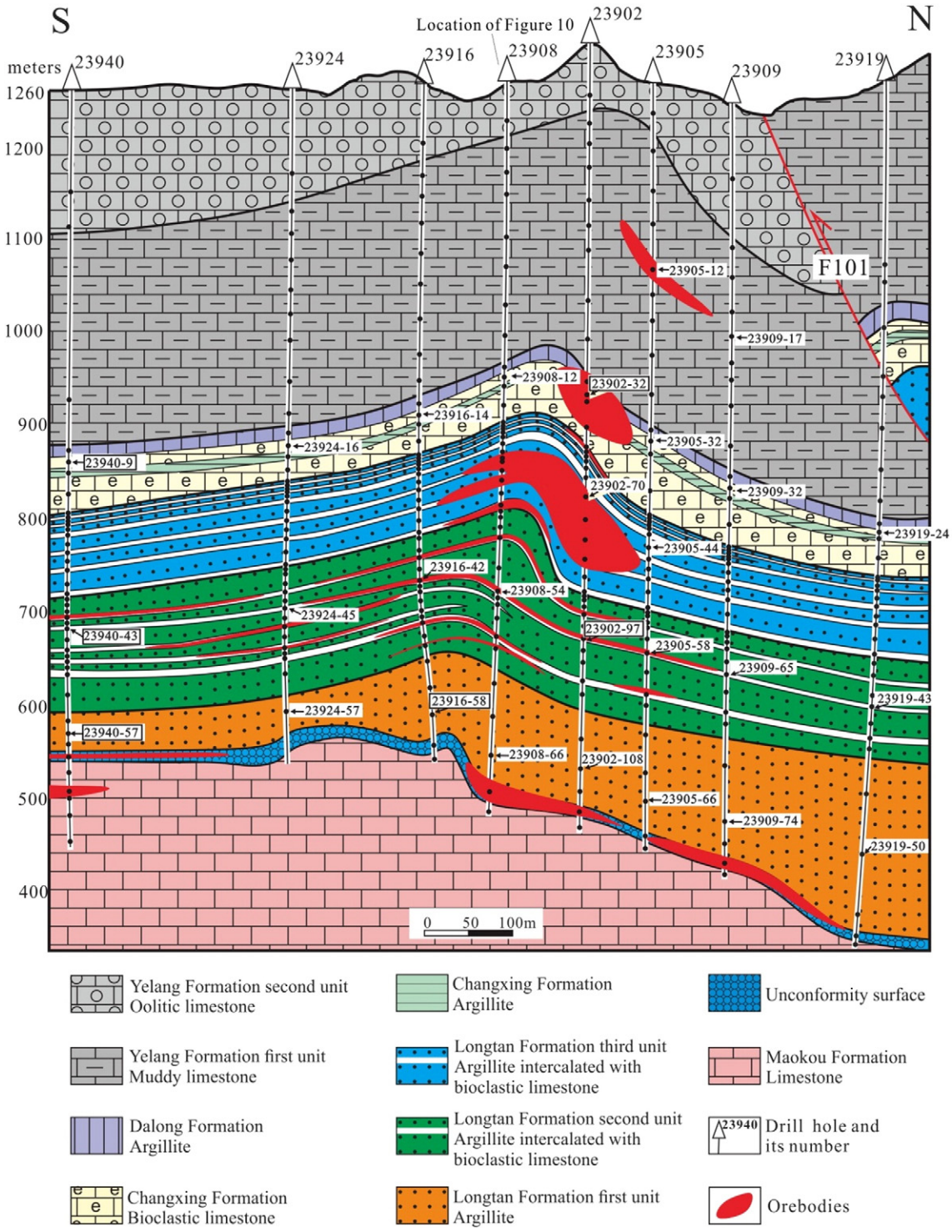

Fig. 3. Geologic N–S cross section through the Shuiyindong mining area (looking west) showing its major structures and stratigraphic units. The position of this cross section is shown in Fig. 2. Locations of analyzed samples are shown by filled dots. Numbers of some samples are not listed because of space limitations. Samples shown with a sample number were analyzed for major elements. Samples with a number within a rectangular frame were chosen for petrographic studies and electron microprobe analyses of arsenian pyrite.

(Fig. 5E, F) and the location of the two samples are shown in Fig. 3. Petrographic studies indicate that minerals in the orebodies (Fig. 5F) and country rocks (Fig. 5E) include arsenian pyrite, quartz, ferroan dolomite, and clay minerals (e.g., illite, chlorite); organic matter also occurs. Large amounts of fine-grained globular and coarse-grained arsenian pyrites occur in the mineralized rock (Fig. 5F), whereas only coarse-grained arsenian pyrites occur in country rock (Fig. 5E). Arsenian pyrites in the orebodies and country rocks are all gold poor (Table 1). Gold-poor arsenian pyrite might have formed because the geochemical conditions that caused pyrite precipitation in argillite were not conducive to the precipitation of gold, or because the consumption of sulfur could not proceed sufficiently to cause the precipitation of gold. Large amounts of chlorite occur in the country rocks but not in the orebodies, which suggests that chlorite was likely consumed by sulfidation reactions. EPMA of organic matter indicate that organic matter in the country rocks does not contain Au, As, Hg, Sb, and S, whereas organic matter in the orebodies contains

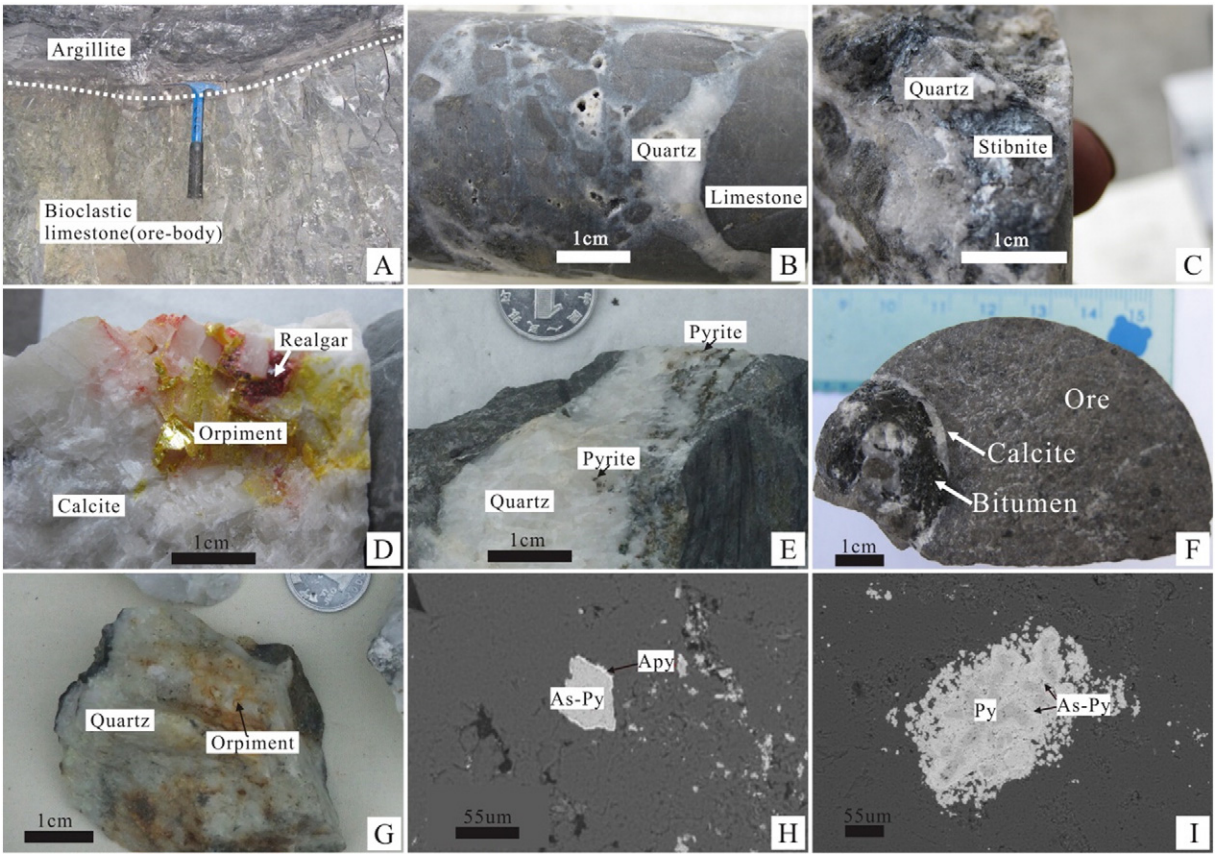

Fig. 4. (A) Photograph of bioclastic limestone layer suffering brittle deformation with many microcracks. (B) Photograph of strongly silicified brecciated limestone from the unconformity surface of the Middle–Upper Permian. (C) Photograph of stibnite in quartz vein. (D) Photograph of realgar and orpiment in calcite vein. (E) Photograph of pyrite in quartz vein. (F) Photograph of bitumen and calcite in ore. (G) Photograph of orpiment in quartz vein. (H) Backscattered electron (BSE) image showing arsenopyrite that occurs as overgrowths on arsenian pyrite. (I) BSE image showing arsenian pyrite forms rims on framboidal pyrite cores. Abbreviations: Apy = arsenopyrite, As-Py = arsenian pyrite, Py = pyrite.

large amounts of these elements (Fig. 5E, F; Table 1). These observations suggest an intergrowth relationship among organic matter, Au, As, Hg, Sb, and S.

5.2. Principal component analyses

Some orebodies occur in the Changxing Formation at the anticlinal core (Fig. 3). Eight samples from the same bioclastic limestone layer of the Changxing Formation were chosen for analyses of major elements (Figs. 3, 6A). The analyses of major elements show that elements such as S, Fe_2O_3, Al_2O_3, TiO_2 and SiO_2 are enriched in the orebodies compared with the country rocks. The content of CaO in the orebodies is less than in the country rocks, and the content of Na_2O is the same between the orebodies and country rocks (Fig. 6A).

The main orebodies at the Shuiyindong gold deposit occur in the bioclastic limestone layers of the Longtan Formation. Eight samples from the same bioclastic limestone layer of the Longtan Formation were chosen for major element analyses (Figs. 3, 6B). These analyses show that S and SiO_2 were enriched in the orebodies, and CaO was depleted from the orebodies. The enrichment of SiO_2 and the depletion of CaO also occurred in the country rocks at the anticlinal flanks, which suggest that the alteration might be more extensive than mineralization. Na_2O is depleted in the orebodies compared with the country rocks, which is similar with the studies of Getchell Carlin-type gold deposit, Nevada (Cail and Cline, 2001). The variations of SiO_2 and Fe_2O_3 from orebodies to country rocks are similar to those of the immobile elements Al_2O_3 and TiO_2. Aluminum and titanium are commonly immobile during alteration and mineralization in Carlin-type deposits (Cail and Cline, 2001; Kesler et al., 2003; Yigit and Hofstra, 2003). Volume loss might have increased the concentration of immobile elements; mass transfer during alteration and mineralization is evaluated further in the next section.

The argillite of the Longtan Formation at the anticlinal core commonly contains lower grade (0.1–1 ppm) orebodies. Eight samples from the same argillite layer of the Longtan Formation first unit were chosen for analyses of major elements (Figs. 3, 6C). The comparison of major elements between the orebodies and country rocks indicates that S was brought into the orebodies and that Na_2O was depleted in the orebodies. The concentrations of elements such as Al_2O_3, TiO_2, Fe_2O_3, CaO, and SiO_2 are all invariant from orebodies to country rocks, which suggests that silicification and decarbonation might have not occurred in the argillite layer of the Longtan Formation first unit.

5.3. Mass transfer associated with alteration and mineralization

Elemental fluxes during alteration and mineralization can be recognized by a comparison of unaltered samples to their strongly mineralized counterparts using immobility isocon diagrams (Gresens, 1967; Grant, 1986). Volume loss due to compaction following the removal of carbonate creates apparent increases in the concentration of immobile elements (Kuehn and Rose, 1992; Cail and Cline, 2001). During the alteration events that add material to the bulk rock, such as silicification and carbonation, immobile elements are diluted. Element immobility and mobility can be identified using X–Y concentration plots that show the concentration of one element versus another for all samples (Finlowbates and Stumpfl, 1981). The highly significant R^2 value of 0.99 for a plot of TiO_2 vs. Al_2O_3 indicates immobile behavior of both elements in sedimentary rocks (Fig. 7A). A similar plot of Zr and Th indicates that these elements are also immobile (Rubin et al., 1993; Cail and Cline, 2001). The regression line of the immobile elements Al_2O_3,

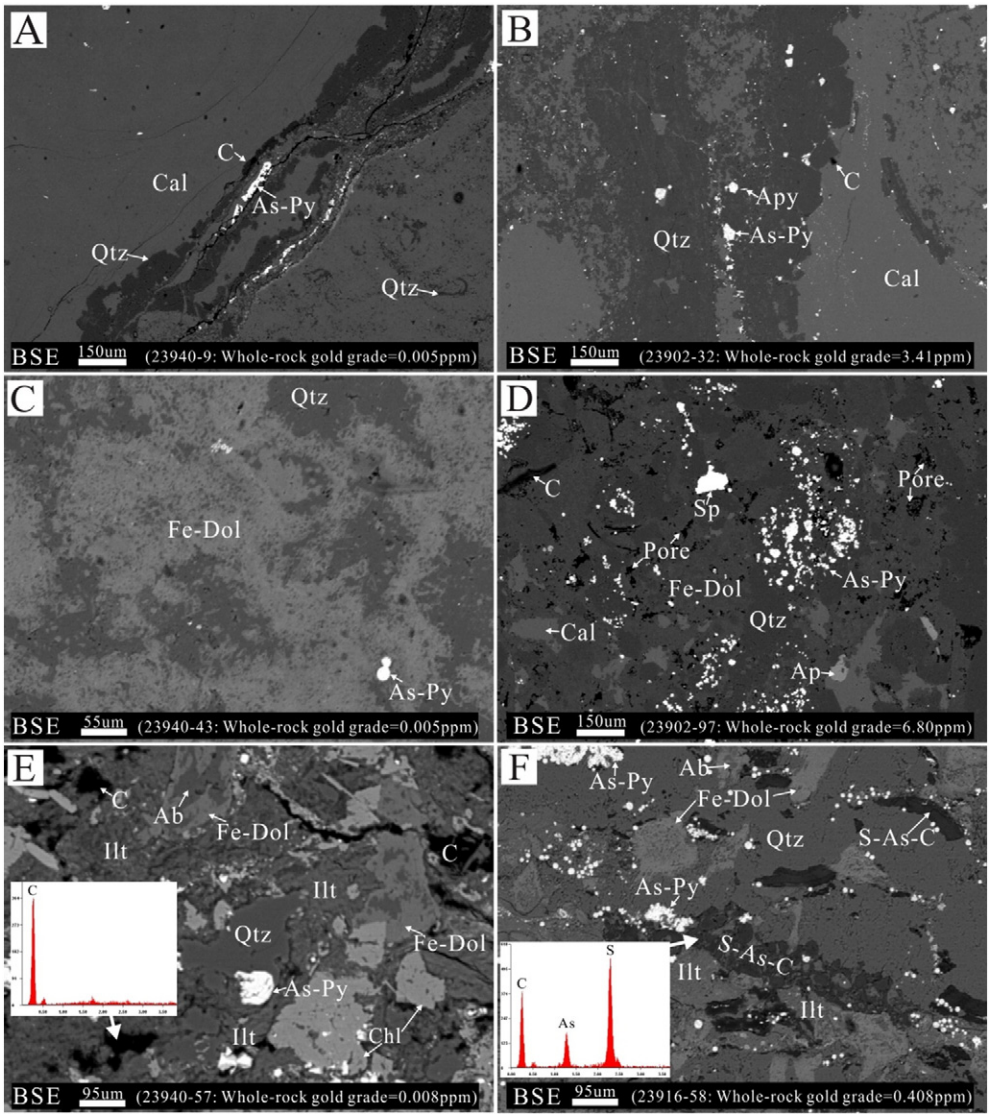

Fig. 5. Back-scattered electron images showing the changes in mineral association between country rocks and orebodies. (A, B) Country rocks and orebodies in the same bioclastic limestone layer of the Changxing Formation. (C, D) Country rocks and orebodies in the same bioclastic limestone layer of the Longtan Formation. (E, F) Country rocks and orebodies in the same argillite layer of the Longtan Formation. Embedded energy dispersive spectrometer images show the chemical composition of organic matter. Abbreviations: Ab = albite, Ap = apatite, Apy = arsenopyrite, As-Py = arsenian pyrite, C = organic matter, Cal = calcite, Chl = chlorite, Dol = dolomite, Fe-Dol = ferroan dolomite, Ilt = Illite, Qz = quartz, S–As–C = organic matter bearing S and As, and Sp = sphalerite.

Table 1
Electron microprobe analyses (wt.%).

Sample no.	Mineral	S	Fe	As	Cu	Sb	Cr	Hg	Au	Total
23940-9	Pyrite	51.5	45.7	0.73	<mdl	<mdl	0.14	<mdl	<mdl	98.1
		51.9	45.6	0.61	<mdl	<mdl	0.52	0.03	<mdl	98.7
23902-32	Pyrite	51.9	45.4	3.12	0.09	<mdl	0.08	0.06	0.08	100.7
		52.3	46.4	0.73	<mdl	<mdl	0.03	<mdl	0.04	99.5
23940-43	Pyrite	51.7	45.5	0.90	0.14	<mdl	0.13	0.05	<mdl	98.4
		52.0	45.7	1.21	<mdl	<mdl	0.06	<mdl	<mdl	99.0
23902-97	Pyrite	50.1	44.4	3.51	0.04	<mdl	0.07	<mdl	0.13	98.3
		52.6	45.2	1.54	0.04	<mdl	0.09	0.03	0.05	99.6
		50.9	44.0	3.39	0.05	<mdl	0.24	<mdl	0.07	98.7
23940-57	Pyrite	53.4	45.8	0.69	<mdl	<mdl	<mdl	<mdl	<mdl	99.9
		52.2	45.5	0.70	0.05	<mdl	0.05	<mdl	<mdl	98.5
		53.9	45.4	0.73	0.07	<mdl	<mdl	<mdl	<mdl	100.1
		53.1	44.6	0.64	0.61	<mdl	<mdl	<mdl	<mdl	99.0
23916-58	Pyrite	52.0	45.5	0.75	0.03	<mdl	0.18	<mdl	<mdl	98.5
		51.7	45.4	0.76	<mdl	0.05	0.15	0.05	<mdl	98.1
		51.9	45.6	0.78	0.06	<mdl	0.14	0.08	<mdl	98.6
	Organic matter	12.0	0.1	4.64	0.01	0.05	0.03	0.21	0.10	17.1
		11.6	0.04	6.07	0.01	0.08	0.02	<mdl	0.43	18.3

mdl: minimum detection limit (Fe: 0.03 wt.%, S: 0.05 wt.%, As: 0.03 wt.%, Cu: 0.03 wt.%, Cr: 0.03 wt.%, Hg: 0.03 wt.%, and Au: 0.04 wt.%).

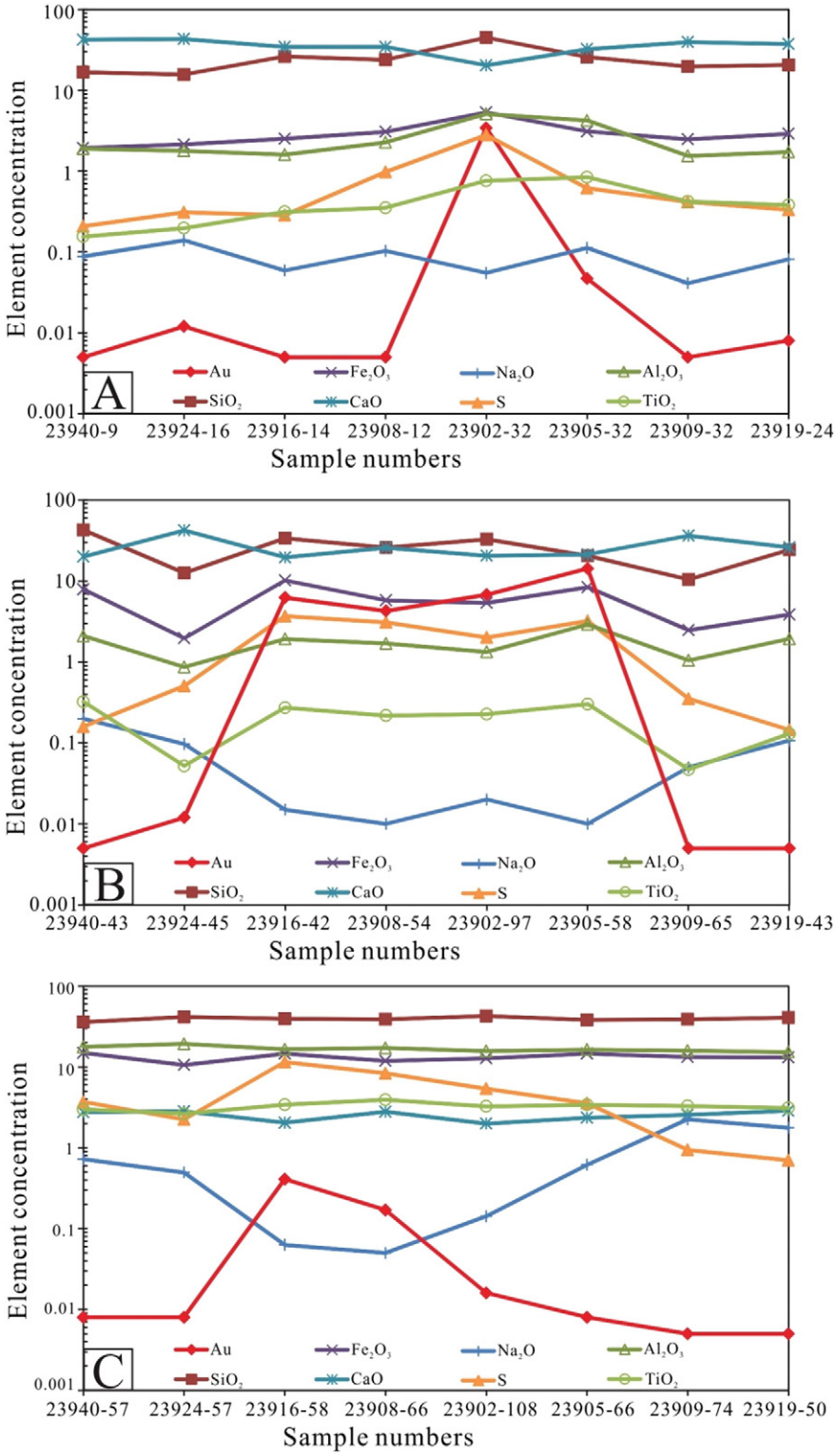

Fig. 6. Variations of major elements in three lithological layers. The locations of the samples are shown in Fig. 3. (A) Bioclastic limestone layer from the Changxing Formation. (B) Bioclastic limestone layer from the Longtan Formation. (C) Argillite layer from the Longtan Formation.

TiO_2, Zr, and Th in the X–Y concentration plots is the immobility isocon. The slope of this straight line defines the mass change during the alteration (Grant, 1986). Elements that lie above the immobility isocon are added to the rock during mineralization and alteration, and elements that lie below the immobility isocon are removed from the rock (Gresens, 1967; Grant, 1986).

The immobility isocon plots in Fig. 7 show addition and loss of elements during alteration and mineralization. The locations of all samples in Fig. 7 are shown in Fig. 3. These samples come from the muddy limestone of the Yelang Formation (23905-12 and 23909-17; Fig. 7B), bioclastic limestone of the Changxing Formation (23902-32 and 23924-16; Fig. 7C), argillite of the Longtan Formation third unit (23902-70 and

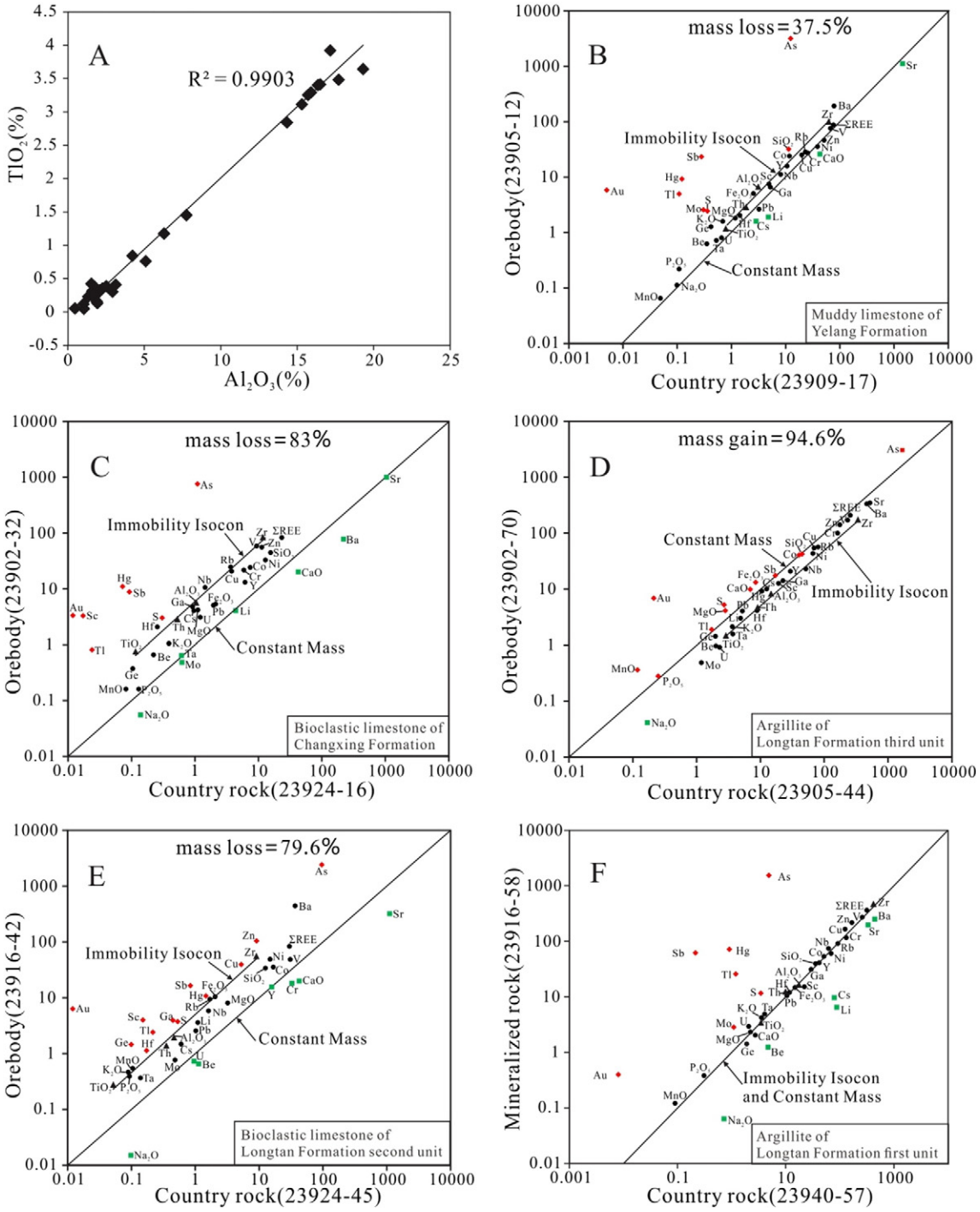

Fig. 7. (A) Correlation plot showing relation between Al_2O_3 and TiO_2. (B–F) Logarithmic isocon plots showing elemental fluxes and mass transfer associated with mineralization between barren samples and mineralized samples. The locations of all samples are shown in Fig. 3. The mass change can be calculated by the equation: $\Delta\text{mass}\ (\%) = (1/m^{-1}) \times 100$, where m is the slope of the immobility isocon (Hofstra, 1994). The immobility isocon is the line of best fit through the concentrations of Al_2O_3, TiO_2, Th, and Zr (filled triangles).

23905-44; Fig. 7D), bioclastic limestone of the Longtan Formation second unit (23916-42 and 23924-45; Fig. 7E), and argillite of the Longtan Formation first unit (23916-58 and 23940-57; Fig. 7F).

The immobility isocon diagrams show that Au, As, Sb, Hg, Tl, and S were significantly added to all mineralized rocks. Detailed EMPA have identified enriched concentrations of Au, As, Sb, and Hg in ore-stage pyrite and organic matter (Table 1), and pyrite and organic matter account for the additions of these elements to mineralized rocks. The site of Tl in ore-stage pyrite and organic matter has not been determined, but given its geochemical similarity to S, pyrite and organic matter is a most likely site. CaO, Na_2O, Sr, and Li were removed from most country rocks (Fig. 7B, C, E) except for the argillite of the Longtan Formation third unit (Fig. 7D), and the loss of these elements are consistent with decarbonation processes typically observed in Carlin-type deposits. The strong loss of CaO indicates that carbonate dissolution was the major process accompanying gold mineralization in these samples. CaO, MgO, Fe_2O_3, SiO_2, and Co were added in the mineralized argillite of the Longtan Formation third unit (Fig. 7D) reflecting the addition of carbonate, pyrite, and quartz; immobile elements were diluted. SiO_2 was added to the mineralized muddy limestone of the Yelang Formation (Fig. 7B) and the mineralized argillite of the Longtan Formation third unit (Fig. 7D), which show obvious silicification in these samples. On

the contrary, SiO_2 remains nearly constant in the main orebodies in the bioclastic limestone (Fig. 7C, E). There is no correlation between gold values and the degree to which the host rocks have undergone silicification. Petrographic studies indicate that orebodies and country rocks in the bioclastic limestone of the Changxing Formation both developed many microcracks that filled with quartz (Fig. 5A, B). The quartz that filled the microcracks of the bioclastic limestone might be from recrystallization of diagenetic quartz. Iron was immobile in most samples except for the argillite (Fig. 7D); and S and As were added to all mineralized samples, which indicates that Fe in the sedimentary rocks combined with the introduced S and As form the arsenian pyrite. The SiO_2, CaO, and Fe_2O_3 were immobile in the argillite (Fig. 7F) which suggests that silicification and decarbonation might have not occurred in the argillite of Longtan Formation first unit. Mo was lost from the mineralized bioclastic limestone of the Changxing Formation (Fig. 7C), whereas the mineralized muddy limestone of the Yelang Formation and the argillite of the Longtan Formation first unit show a significant gain of Mo (Fig. 7B, F). Sc was significantly gained in mineralized bioclastic limestone (Fig. 7C, E). Carbonate or bicarbonate complexes of Sc could be of potential importance for Sc enrichment substituting for Mg and Fe ion (Eby, 1973; Bogoch et al., 1984). Substantial Sc could be transported at moderately acidic conditions (Wood and Samson, 2006). The ore-forming fluid from the Shuiyindong deposit was of low-intermediate temperature type, low salinity, mildly acidic, low oxygen fugacity, and highly reduced (Su, 2002; Su et al., 2009a). Thus, it is intelligible that Sc was enriched in mineralized bioclastic limestone. Fig. 7E show small gains of Zn, Cu, Ga, and Ge in the mineralized bioclastic limestone of the Longtan Formation second unit, and the enrichment of zinc is associated with the introduction of sphalerite (Fig. 4D).

The question of whether sulfur and iron were introduced into orebodies together or independently can be tested effectively with the iron and sulfur contents of all samples (Stenger et al., 1998). Fe and S contents of the rocks have been normalized to Al contents (Hofstra and Cline, 2000). Fig. 8 shows Fe/Al vs. S/Al relations for different grade samples and a pyrite line marking the relative concentrations of these elements in pyrite $S = 1.15 \times Fe$ (in wt.%) (Stenger et al., 1998). The distribution of all samples below the pyrite line suggests that the sedimentary rocks contain more iron than is needed to combine with all of their contained sulfur to form pyrite. Iron-bearing carbonate minerals are found in almost all samples (Fig. 5). Low-grade samples plot in a cluster in the lower part of the pyrite line and extending downward toward the Fe/Al axis. The black arrows in Fig. 8 show paths that would be followed by samples that underwent pyritization or sulfidation. The latter process might be the principal mechanism of gold precipitation.

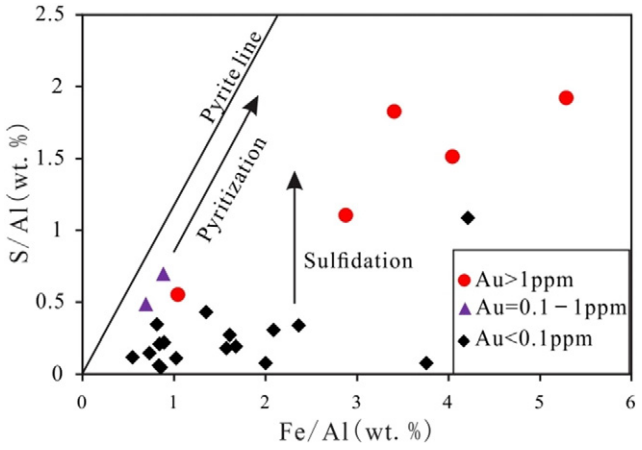

Fig. 8. Correlation diagrams showing relations between iron and total sulfur both normalized to immobile Al in different grade samples. These samples are marked with a sample number in Fig. 3. Arrows show direction of compositional change associated with pyritization (addition of sulfur and iron) and sulfidation (addition of only sulfur).

5.4. Spatial distribution of gold and related elements

Carlin-type gold deposits in Guizhou are characteristically rich in As, Sb, Hg, and Tl (Hu et al., 2002; Xia, 2005; Peters et al., 2007; Su et al., 2009a). The spatial distributions of Au, As, Sb, Hg, Tl, and Li in the representative N–S cross section and their relations to the stratigraphic and structural features are shown in Fig. 9. The spatial distributions of Au, As, Sb, Hg, and Tl are roughly similar, and are arranged along the unconformity surface and the anticlinal axis, which indicates roughly positive correlations among these elements (Fig. 9). The distributions of ore-forming elements might reflect the pathways of ore-forming fluids ascending from the deep to shallow crust and might also reflect local processes and controls.

Fig. 9 shows that Au, As, Sb, Hg, and Tl appear roughly zoned, from bottom to top, in the order: Sb–Tl–As–Hg–Au–Hg–As. In this profile, arsenic is the most widely distributed element, similar to the Twin Creeks deposit, Nevada (Stenger et al., 1998). The presence of some gold-poor areas with enriched arsenic values in the upper part of the section is consistent with the element's use as an indicator element for gold exploration (Arehart, 1996). Antimony deposits and mercury deposits often exist around Carlin-type gold deposits in Guizhou (Fig. 1). In fact, most of the gold deposits shown in Fig. 1 were found by exploration in, or near, known deposits and occurrences of Hg, Sb, As, and Tl (Cunningham et al., 1988; Ashley et al., 1991; Peters et al., 2007).

The distribution of Li, which shows an apparent absence in the Longtan Formation at the anticlinal core (Fig. 9F), contrasts with the distribution of Au, As, Sb, Hg, and Tl. The unique character of Li might indicate that the ore-forming fluids interacted with strata during the process of upward migration and that Li was removed. Li might form an enriched cap over the ore-bearing horizon; therefore, Li could be used as an effective ore-indicator element.

Different host rocks have been preferentially mineralized by different elements. The bioclastic limestone is commonly enriched in Au, whereas the argillite is enriched in As and Hg (Fig. 9). Sb and Tl are obviously enriched at the unconformity surface. To illustrate further the spatial distribution difference of Au, As, Sb, Hg, and Tl, the second and third units of the Longtan Formation in drill hole 23908 were selected for additional study (Fig. 10). The trend lines of Au, As, Sb, Hg, and Tl in the second and third units of the Longtan Formation indicate inconsistencies in the distribution of these elements. The samples with Au content greater than 1 ppm are all located in bioclastic limestone, but their contents of As, Sb, Hg, and Tl are less than those in the surrounding argillite. The samples with Au content around 0.1 ppm are mostly located in argillite, and their contents of As, Sb, Hg, and Tl are relatively greater than those in the surrounding limestone. The samples with an Au content of less than 0.01 ppm are all located in bioclastic limestone and these samples have the lowest contents of As, Sb, Hg, and Tl. He (1996) reported differential enrichment of As and Au and attributed it to changing physicochemical conditions during hydrothermal evolution. Au and As were transported in fundamentally different ways in hydrothermal fluids, Au is complexed by bisulfide (Seward, 1973, 1984), As is behaving as a weak acid and forming various As complexes (Heinrich and Eadington, 1986), which might have resulted in the differential behavior of these elements.

5.5. Spatial distribution of trace elements

A correlation matrix calculated using the 350 samples (Table 2) shows the interrelationships of all trace elements. The correlation coefficients between any two of Be, Sc, V, Cr, Co, Ni, Cu, Zn, Ga, Ge, Y, Zr, Nb, ΣREE, Hf, Ta, Pb, Th, and Rb are all greater than 0.5, and the correlation

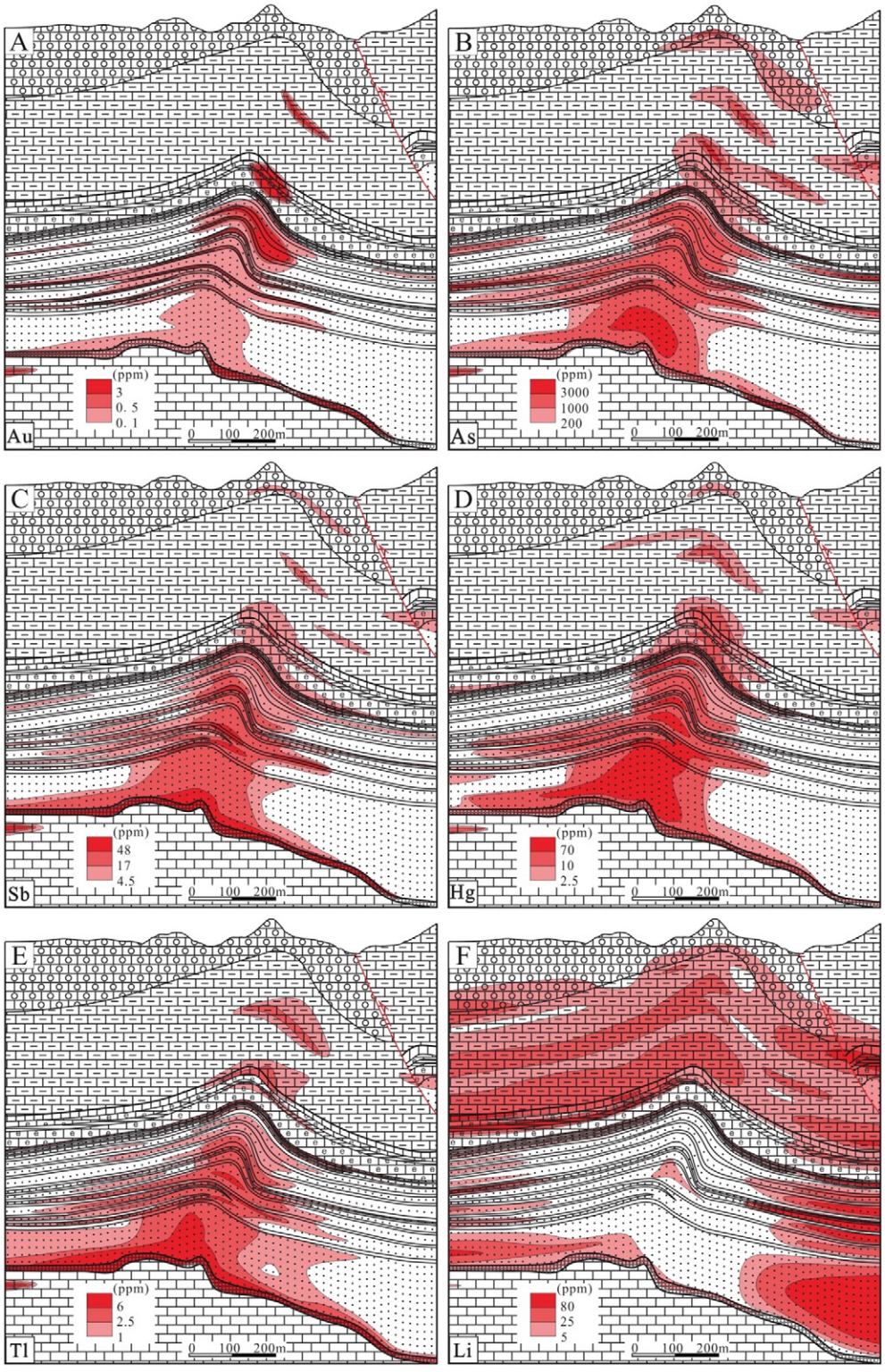

Fig. 9. Spatial distributions of Au, As, Sb, Hg, Tl, and Li along the N–S cross section and their relations to stratigraphy and structures.

coefficients of Mo and U are also greater than 0.5. Among the ore-related elements, Sb shows best the correlation with Au grade (Table 2). Au does not show a close correlation with As, Hg, and Tl, and this indicates the spatial differences among these elements. The spatial distributions of elements with correlation coefficients greater than 0.5 are roughly similar and can be shown in one graph using a new variable.

Factor analysis is a method used to reduce a large data set to a smaller number of variables (Theodore et al., 2003). The method produces a small set of variables called factors or principal components that summarizes the essential information of the original larger set of observations. These factors can be interpreted in terms of the various geochemical components in the original samples. In this study, 6 independent components

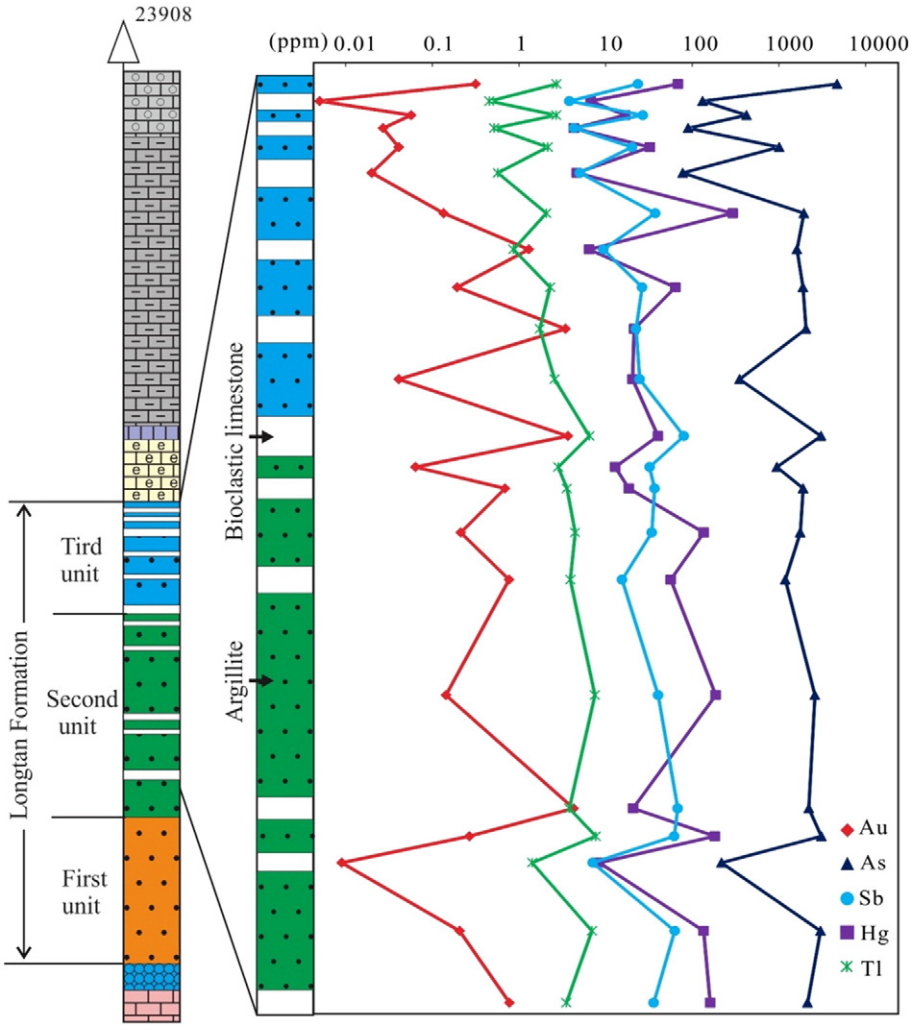

Fig. 10. Variation of Au, As, Sb, Hg, and Tl in a selected part of drillhole 23908. The drillhole location is shown in Fig. 3.

(factors) accounting for 80.82% of the total variance were extracted from 43 elements using SPSS (IBM SPSS, NY, USA) software, and the results are shown in Table 3. Each factor score is the sum of the products of the samples' observed values and their corresponding factor loading.

The scores were contoured for each of the six factors to examine the spatial distribution of the values (Fig. 11). Factor 1 has strong positive correlations with Zr, Hf, Ta, ΣREE, Y, Th, Nb, Ga, Be, Zn, Rb, Sc, Cu, V, Ge, Pb, and Cs, and factor 6 has strong positive correlations with Ba and Sr. The scores for factors 1 and 6 show strong stratigraphic control, and therefore these may be related to a premineralization district-scale sedimentation factor. The scores of factor 2, which have high correlations with Co, Cr, and Ni, are enriched in the Longtan Formation along the anticline axis suggesting that this factor might represent enrichment during deformation or mineralization. Factor 3 has strong positive correlations with Au, As, Sb, and Tl, and factor 5 has a strong negative correlation with Li and positive correlations with As and Hg, which suggests that factors 3 and 5 represent mineralization. The scores of factor 4, which have positive correlations with Mo and U, are relatively enriched in the unconformity surface compared with the surrounding limestone and argillite. Hu et al. (2002) and Zhang et al. (2003) indicated that U is also one of the anomalous elements in the Carlin-type gold deposits of Guizhou. However, the distribution of the enriched scores of factor 4 is not terribly similar to the distribution of ore-related elements in Fig. 11, so we are not sure that this factor represents gold mineralization. U–Mo enrichment may be unrelated to Au mineralization, and may record another hydrothermal fluid flow event which is not discussed or evaluated before.

6. Discussion

6.1. Precipitation mechanisms of gold and related elements

Integrated geologic, geochemical, fluid-inclusion, and stable isotope studies have established that sulfidation, decarbonation, cooling, and fluid mixing are the most important factors controlling the formation of Carlin-type gold deposits in Nevada (Seward, 1984; Hofstra et al., 1991, 2003; Kuehn and Rose, 1995; Arehart, 1996; Stenger et al., 1998; Simon et al., 1999a; Cail and Cline, 2001; Fortuna et al., 2003; Kesler et al., 2003; Yigit and Hofstra, 2003). Decarbonation and sulfidation are the most common types of rock alteration seen in many Carlin-type deposits (Arehart, 1996; Hofstra and Cline, 2000; Cline et al., 2005). The conclusions of this research were derived largely from comparisons of unaltered samples to their strongly mineralized counterparts based on geochemical data, and these comparisons provide useful insights into the precipitation processes of gold and related elements at the Shuiyindong gold deposit.

6.1.1. Role of sulfidation and decarbonation in deposition of gold ores

Petrographic studies (Fig. 5D) indicate that the ferroan dolomite in the bioclastic limestone layer of the Longtan Formation has been partially dissolved and left many pores. In the orebodies (Fig. 5B, D, F), a large amount of gold-bearing arsenian pyrite (Table 1) is concentrated along the quartz boundaries or included in the quartz grains, whereas only small amounts of gold-poor arsenian pyrite (Table 1) occur in country

Table 2
Trace element correlation coefficients.

	Au	As	Hg	Sb	Tl	Li	Be	Sc	V	Cr	Co	Ni	Cu	Zn	Ga	Ge	Rb	Sr	Y	Zr	Nb	Mo	Cs	Ba	∑REE	Hf	Ta	Pb	Th	U
Au	1.00																													
As	0.39	1.00																												
Hg	0.13	0.48	1.00																											
Sb	**0.61**	0.35	0.24	1.00																										
Tl	0.19	0.28	0.19	**0.60**	1.00																									
Li	−0.09	−0.14	−0.13	−0.08	−0.05	1.00																								
Be	−0.11	0.00	0.07	−0.06	0.01	0.32	1.00																							
Sc	−0.09	0.17	0.31	−0.01	0.03	0.26	**0.81**	1.00																						
V	−0.09	0.19	0.31	0.02	0.11	0.23	**0.76**	**0.94**	1.00																					
Cr	−0.09	0.14	0.21	−0.01	0.04	0.14	**0.52**	**0.72**	**0.83**	1.00																				
Co	0.00	0.21	0.27	0.06	0.12	0.14	**0.54**	**0.70**	**0.73**	**0.60**	1.00																			
Ni	−0.08	0.08	0.13	−0.09	−0.03	0.15	**0.53**	**0.68**	**0.69**	**0.67**	**0.60**	1.00																		
Cu	0.00	0.20	0.39	0.06	0.10	0.25	**0.75**	**0.87**	**0.86**	**0.57**	**0.70**	**0.60**	1.00																	
Zn	−0.03	0.19	0.31	0.07	0.09	0.25	**0.85**	**0.87**	**0.86**	**0.67**	**0.65**	**0.65**	**0.81**	1.00																
Ga	−0.07	0.20	0.32	0.03	0.13	0.25	**0.85**	**0.92**	**0.91**	**0.67**	**0.70**	**0.63**	**0.89**	**0.92**	1.00															
Ge	−0.06	0.21	0.23	0.07	0.15	0.14	**0.71**	**0.78**	**0.77**	**0.59**	**0.62**	**0.50**	**0.73**	**0.78**	**0.80**	1.00														
Rb	−0.03	0.21	0.29	0.03	0.13	0.16	**0.83**	**0.90**	**0.88**	**0.63**	**0.69**	**0.66**	**0.83**	**0.88**	**0.94**	**0.76**	1.00													
Sr	0.03	−0.14	−0.25	−0.11	−0.10	0.00	−0.37	−0.42	−0.41	−0.33	−0.32	−0.18	−0.37	−0.43	−0.39	−0.37	−0.37	1.00												
Y	−0.09	0.19	0.30	0.02	0.10	0.18	**0.85**	**0.81**	**0.79**	**0.58**	**0.60**	**0.52**	**0.78**	**0.88**	**0.93**	**0.75**	**0.84**	−0.38	1.00											
Zr	−0.07	0.19	0.29	0.03	0.14	0.21	**0.86**	**0.85**	**0.84**	**0.61**	**0.64**	**0.58**	**0.82**	**0.91**	**0.97**	**0.77**	**0.89**	−0.38	**0.97**	1.00										
Nb	−0.07	0.19	0.28	0.08	0.24	0.20	**0.83**	**0.83**	**0.84**	**0.63**	**0.64**	**0.55**	**0.81**	**0.89**	**0.95**	**0.78**	**0.86**	−0.37	**0.94**	**0.98**	1.00									
Mo	−0.02	0.06	0.02	0.02	0.05	−0.02	0.01	−0.04	0.14	0.39	0.03	0.21	−0.03	0.08	0.03	−0.02	0.00	−0.09	0.08	0.06	0.04	1.00								
Cs	−0.10	0.00	0.11	−0.06	−0.01	0.43	**0.77**	**0.72**	**0.69**	0.44	0.48	0.43	**0.70**	**0.69**	**0.72**	**0.57**	**0.71**	−0.35	**0.68**	**0.70**	**0.68**	−0.03	1.00							
Ba	−0.01	0.15	0.10	0.11	0.23	0.04	0.15	0.18	0.23	0.18	0.31	0.15	0.23	0.20	0.24	0.22	0.21	0.17	0.22	0.24	0.27	−0.01	0.12	1.00						
∑REE	−0.07	0.20	0.29	0.02	0.13	0.20	**0.84**	**0.82**	**0.82**	**0.61**	**0.64**	**0.56**	**0.80**	**0.89**	**0.95**	**0.77**	**0.86**	−0.34	**0.97**	**0.99**	**0.97**	0.08	**0.67**	0.25	1.00					
Hf	−0.07	0.17	0.27	0.03	0.13	0.20	**0.85**	**0.81**	**0.81**	**0.59**	**0.61**	**0.55**	**0.79**	**0.89**	**0.95**	**0.75**	**0.86**	−0.37	**0.97**	**1.00**	**0.97**	0.08	**0.68**	0.23	**0.98**	1.00				
Ta	−0.09	0.16	0.27	0.03	0.15	0.19	**0.85**	**0.81**	**0.80**	**0.59**	**0.60**	**0.53**	**0.78**	**0.90**	**0.94**	**0.77**	**0.85**	−0.41	**0.95**	**0.98**	**0.97**	0.07	**0.68**	0.22	**0.97**	**0.98**	1.00			
Pb	0.11	0.19	0.20	0.12	0.11	0.19	**0.66**	**0.64**	**0.64**	0.46	**0.55**	**0.61**	**0.71**	**0.68**	**0.77**	**0.58**	**0.75**	−0.19	**0.75**	**0.78**	**0.74**	0.16	**0.54**	0.18	**0.78**	**0.79**	**0.74**	1.00		
Th	−0.06	0.17	0.25	0.02	0.12	0.21	**0.83**	**0.78**	**0.76**	**0.54**	**0.58**	**0.56**	**0.77**	**0.87**	**0.93**	**0.73**	**0.87**	−0.29	**0.94**	**0.97**	**0.93**	0.10	**0.63**	0.21	**0.96**	**0.98**	**0.95**	**0.84**	1.00	
U	−0.04	0.12	0.10	0.03	0.12	−0.01	0.20	0.13	0.22	0.31	0.14	0.19	0.16	0.21	0.29	0.14	0.21	−0.08	0.36	0.35	0.33	**0.57**	0.11	0.03	0.38	0.38	0.35	0.45	0.40	1.00

Table 3
Rotated (varimax) factor-loading matrix.

Element	Factor 1	Factor 2	Factor 3	Factor 4	Factor 5	Factor 6
Zr	**0.98**	0.12	0.03	0.10	0.05	0.01
Hf	**0.98**	0.08	0.02	0.14	0.04	0.01
Ta	**0.97**	0.07	0.02	0.11	0.05	−0.02
REE	**0.97**	0.11	0.02	0.13	0.06	0.04
Y	**0.96**	0.08	0.01	0.12	0.08	−0.01
Th	**0.96**	0.05	0.02	0.18	0.02	0.05
Nb	**0.96**	0.13	0.08	0.08	0.05	0.05
Ga	**0.95**	0.27	0.04	0.02	0.03	0.00
Be	**0.89**	0.14	−0.07	−0.02	−0.21	−0.09
Zn	**0.88**	0.32	0.06	0.02	0.01	−0.08
Rb	**0.88**	0.33	0.05	−0.03	0.05	−0.01
Sc	**0.82**	0.47	−0.02	−0.12	0.01	−0.09
Cu	**0.81**	0.39	0.09	−0.11	0.04	−0.03
V	**0.78**	**0.56**	0.02	0.03	0.03	−0.04
Ge	**0.77**	0.30	0.07	−0.09	0.09	−0.01
Pb	**0.77**	0.13	0.15	0.27	−0.05	0.09
Cs	**0.73**	0.22	−0.03	−0.12	−0.32	−0.15
Co	**0.58**	**0.57**	0.08	−0.06	0.10	0.12
Cr	**0.49**	**0.70**	−0.03	0.30	0.04	−0.04
Ni	**0.48**	**0.66**	−0.10	0.17	−0.05	0.07
Sb	0.01	−0.04	**0.90**	0.01	0.04	−0.01
Au	−0.09	0.04	**0.77**	−0.03	0.02	−0.09
Tl	0.13	−0.10	**0.67**	0.08	0.08	0.20
As	0.13	0.17	**0.52**	0.01	**0.50**	0.00
Mo	−0.06	0.28	0.03	**0.87**	−0.02	−0.08
U	0.30	−0.10	0.03	**0.84**	0.07	0.03
Li	0.24	0.15	0.04	−0.09	**−0.75**	−0.02
Hg	0.25	0.18	0.25	−0.07	**0.64**	−0.09
Ba	0.21	0.18	0.13	−0.06	0.08	**0.81**
Sr	−0.36	−0.19	−0.09	0.02	−0.18	**0.67**

Extraction method: principal component analysis.
Rotation method: varimax with Kaiser normalization.
Rotation converged in six iterations.

rocks (Fig. 5A, C, E). Petrographic and EMPA studies indicate that gold in the primary ores occurs mainly in the arsenian pyrite. The principal component analyses (Fig. 6) show that the content of CaO in the orebodies is less than in the country rocks. The variations of Fe_2O_3 and SiO_2 from orebodies to country rocks are not consistent with the variation of S, but with the immobile elements, such as Al_2O_3 and TiO_2 (Fig. 6B). Mass transfer calculations show that Fe_2O_3 and SiO_2 are immobile in the main orebodies hosted in bioclastic limestone (Fig. 7C, E), and CaO was removed. The relations between Fe and S (Fig. 8) indicate that the sedimentary rocks at the Shuiyindong deposit contain more iron than is needed to combine with all of their contained sulfur to form pyrite. Su et al. (2009a) concluded that the original ore-forming fluids were Fe poor, but that they were possibly sulfur rich. Thus, the main orebodies hosted by the bioclastic limestone at the Shuiyindong deposit have undergone sulfidation and decarbonation. The iron that underwent sulfidation might have been derived from ferroan dolomite, which released it into solution because of decarbonation. Ore-forming fluids at the Shuiyindong gold deposit contained up to 4 mol% CO_2 (Su et al., 2009a), which was likely the principal acid volatile in the ore-forming fluids promoting the dissolution of ferroan dolomite in the host rocks (Muntean et al., 2011). The addition of iron to the argillite (Fig. 7D) indicates that pyritization (addition of sulfur and iron) occurred in addition to sulfidation (addition of only sulfur). This pyritization might be a different manifestation of the sulfidation or be an unrelated event to the other sulfidation processes. The iron that underwent pyritization might have been derived largely from underlying or surrounding ferroan dolomite.

6.1.2. Deposition of As, Sb, Hg: cooling and organic matter role

Hg, Sb, and As commonly formed sulfide minerals, such as stibnite, realgar, and orpiment, in late-stage quartz–calcite veins in the unconformity surface and in reverse faults (Fig. 4C, D, G). Stibnite deposition was controlled mainly by cooling, typically to less than 250 °C (Williams-Jones and Norman, 1997; An and Zhu, 2010). Quartz, stibnite, orpiment, and realgar have prograde solubility, and they presumably precipitated in fractures as the fluids cooled during the latter stages of the hydrothermal systems (Hu et al., 2002). Thus, fluid cooling might account for the deposition of stibnite, realgar, and orpimentin in late-stage quartz–calcite veins, although such factors as pH and oxidation state of the system are also involved.

As, Sb, and Hg also occur as intergrowths with organic matter in argillite. Petrographic studies (Fig. 5E, F) and chemical analyses of organic matter (Table 1) show that organic matter in the mineralized argillite contains large amounts of Au, As, Sb, Hg, and S, but organic matter in unaltered argillite does not contain these elements. Studies of reactions between carbonaceous materials and gold-bearing solutions show that the rocks contain an activated carbon component capable of adsorbing gold chloride or gold cyanide complexes from solution (Radtke and Scheiner, 1970). The enrichment of As, Sb, and Hg in the argillite of the Longtan Formation (Figs. 9, 10) may be related to substantial amounts of organic matter in the argillite. The organic carbon was present in the rocks prior to gold deposition. The organic matter likely served as a chemical trap (reductant) for the ore fluids, causing the precipitation of Au, As, Sb, Hg, and S in organic matter. These elements might then form discrete minerals that are inclusions in the organic matter.

A mixture of high-molecular-weight hydrocarbons usually associated with the activated carbon components in the Carlin gold deposit, Nevada (Radtke and Scheiner, 1970). Carbonaceous material at the Carlin deposit, referred to as bituminous hydrocarbon, was accumulated in various types of open spaces in the rocks and was remobilized accompanying and following hydrothermal mineralization (Hausen, 1967). Bitumen in the Shuiyindong deposit is commonly present as a migrated hydrocarbon product in mineralized rocks (Fig. 4F), but is absent in barren sedimentary rocks. Fluid inclusions in the main ore-forming stage of the Shuiyindong gold deposit are dominated by aqueous inclusions as well as hydrocarbon-rich inclusions (Su, 2002). These observations suggest an intimate relationship between bitumen precipitation and gold mineralization (Zhuang et al., 1999; Gu et al., 2012).

6.2. Migration paths of ore-forming fluids

Deposit-scale distributions of gold and related elements can reflect the passage of fluids through the rocks. The spatial distributions of gold and related elements in the representative cross section show that the ore-forming fluids migrated along the unconformity surface and the anticline axis, rather than being randomly dispersed (Fig. 9). The anticline axis acted as the upwelling channel of the ore-forming fluids at the Shuiyindong gold deposit.

The unconformity surface is enriched in Au, As, Sb, Hg, and Tl (Fig. 9). The migration of ore-forming fluids at the unconformity surface also formed some gold or antimony deposits. For example, the Dachang antimony deposit and the Getang gold deposit occur at the unconformity surface (Zhang et al., 2003; Peters et al., 2007). Therefore, the unconformity surface not only acted as a migration channel for ore-forming fluids, but also as a trap for ore-forming elements.

The second and third units of the Longtan Formation consist of argillite with interlayered bioclastic limestone. Bioclastic limestone commonly has high porosity, and the dissolution of carbonate can further increase both its porosity and its permeability (Bloomstein et al., 1991; Kuehn and Rose, 1992). Furthermore, competent bioclastic limestone layers tend to suffer brittle deformation during anticline formation (Fig. 4A), which further increases the permeability of those layers (Peters, 2004). Bioclastic limestone layers with both high porosity and high permeability contributed to the lateral migration of ore-forming fluids and their interaction with the bioclastic limestone layers. Thus, in the second and third units of the Longtan Formation, orebodies extend substantial distances along the bioclastic limestone layers (Fig. 9A).

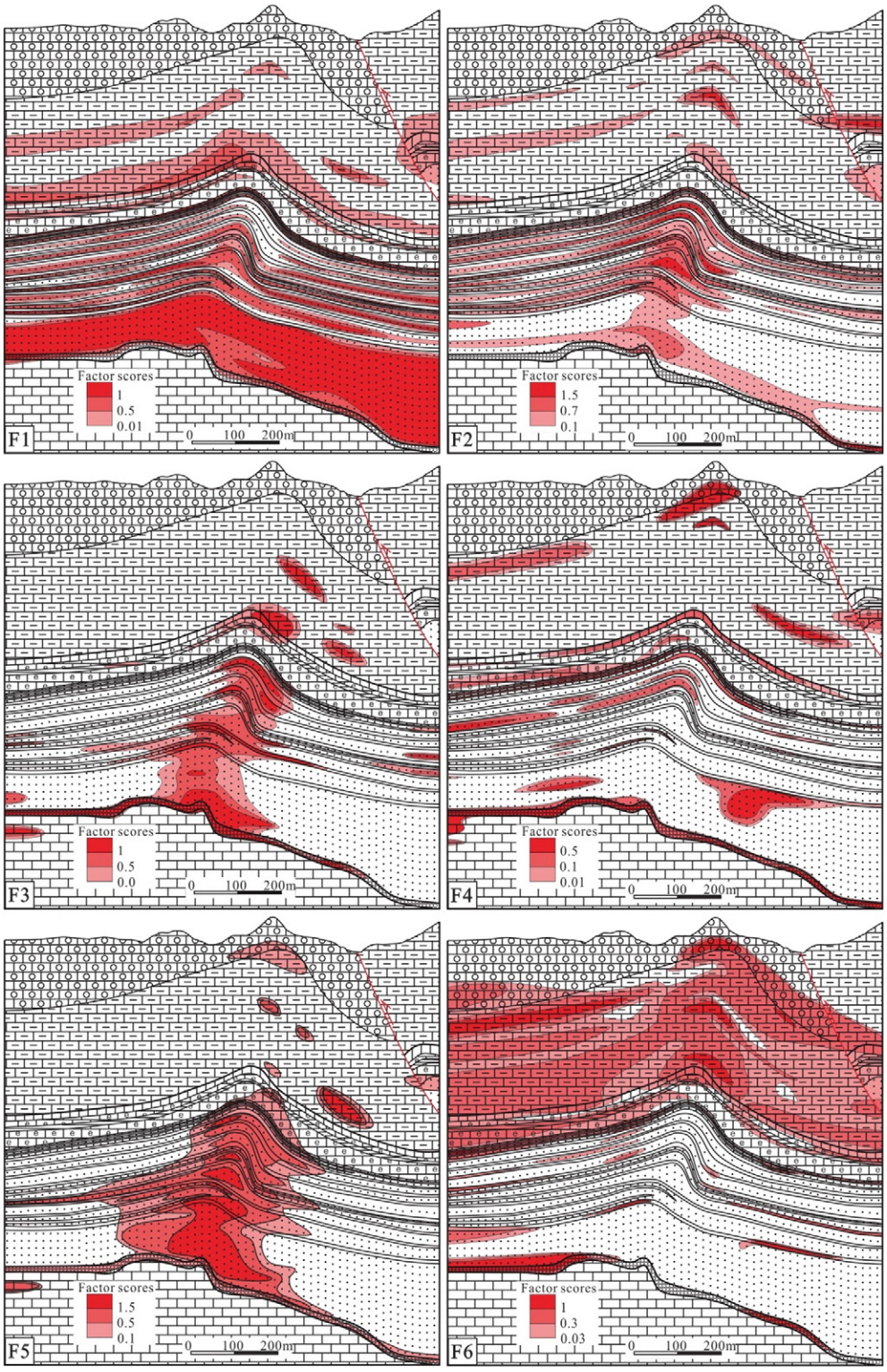

Fig. 11. Spatial distribution maps of factor scores along the N–S cross section showing their relations to stratigraphic and structural features. (F1) Zr, Hf, Ta, ∑REE, Y, Th, Nb, Ga, Be, Zn, Rb, Sc, Cu, V, Ge, Pb, and Cs; (F2) Co, Cr, and Ni; (F3) Au, As, Sb, and Tl; (F4) Mo and U; (F5) As, Hg, and −Li; and (F6) Ba and Sr.

7. Conclusions

Integrated petrographic studies, EMPA, isocon diagrams, Fe–S relations, and deposit-scale distributions of Au, As, Sb, Hg, Tl, and trace elements have provided insight into the precipitation mechanisms of minerals, or elements from fluids, and the migration paths of ore-forming fluids at the Shuiyindong Carlin-type gold deposit. The main conclusions are summarized below.

Mass transfer calculations show that Au, As, Sb, Hg, Tl, and S were significantly added to all mineralized rocks, Fe_2O_3 and SiO_2 were immobile in the main orebodies hosted in bioclastic limestone, and CaO, Na_2O, Sr, and Li were removed from country rocks. Petrographic studies indicate

that the ferroan dolomite in the bioclastic limestone layer of the Longtan Formation was partially dissolved, which increased porosity. Element fluxes and petrographic observations show that sulfidation and decarbonation are spatially associated with gold mineralization. Hg, Sb, and As commonly formed sulfide minerals, such as stibnite, realgar, and orpiment, in late-stage quartz–calcite veins, or absorbed by organic matter in argillite. Fluid cooling presumably led to the deposition of stibnite, realgar, and orpiment in the late-stage quartz–calcite veins at the Shuiyindong gold deposit. Organic matter likely served as a reductant in argillite for the ore fluids, causing the precipitation of As, Sb, Hg, and S, as well as Au.

The migration paths of the ore-forming fluids were identified using the deposit-scale distributions of gold and related elements. Rock strata and structures allowed the ore-forming fluids to migrate horizontally along the unconformity surface of the Middle–Upper Permian, converge on the high position of an anticline, and then ascend into the overlying strata along the anticline axis. The distributions of the major and trace elements show that elements that accompanied the ore-forming fluids include Au, As, Sb, Hg, Tl, and S, and that Na_2O and Li were depleted in the Longtan Formation at the anticline core during gold mineralization. The enrichment of Co, Cr, and Ni in the Longtan Formation at the anticline core might be associated with deformation during anticline formation, or with the mineralization of gold. Different host rocks were preferentially mineralized by different elements. The bioclastic limestone is commonly enriched in Au, whereas the argillite is enriched in As, Hg, Sb, and Tl. The zonation of ore-forming elements in the deposit appears to be Sb–Tl–As–Hg–Au–Hg–As (from bottom to top).

Our results indicate that anticlines that fold the Middle–Upper Permian unconformity are favorable locations for the Carlin-type gold deposits in Guizhou, China. Bioclastic limestone is the favorable host for the precipitation of Au. Anomalies of As and Hg in soil or stream sediments might be important indicators, and these elements can be used as indicator elements for exploration for new Carlin-type gold orebodies in Guizhou Province.

Acknowledgments

We are grateful to the Guizhou Zijin gold mine for access to the mine and to Xing-Chun, Zhang, Jian-Zhong Liu, Jie Qi, and Ze-Peng Wang for geological guidance and discussions during the studies. The project was supported financially by the Major State Basic Research Development Program of China (973 Program) (2014CB440905) and the 12th Five-Year Plan Project of the State Key Laboratory of Ore-deposit Geochemistry, Chinese Academy of Sciences (SKLODG-ZY125-01). We thank the Editor-in-Chief Prof. Franco Pirajno and associate editor Jeffrey L Mauk and reviewers for their constructive comments and helpful suggestions.

Appendix A. Supplementary data

Supplementary data to this article can be found online at http://dx.doi.org/10.1016/j.oregeorev.2015.02.006.

References

An, F., Zhu, Y.F., 2010. Native antimony in the Baogutu gold deposit (west Junggar, NW China): its occurrence and origin. Ore Geol. Rev. 37 (3), 214–223.
Arehart, G.B., 1996. Characteristics and origin of sediment-hosted disseminated gold deposits: a review. Ore Geol. Rev. 11 (6), 383–403.
Arehart, G.B., Donelick, R.A., 2006. Thermal and isotopic profiling of the pipeline hydrothermal system: application to exploration for Carlin-type gold deposits. J. Geochem. Explor. 91 (1–3), 27–40.
Arehart, G.B., Eldridge, C.S., Chryssoulis, S.L., Kesler, S.E., 1993. Ion microprobe determination of sulfur isotope variations in iron sulfides from the Post/Betze sediment-hosted disseminated gold deposit, Nevada, USA. Geochim. Cosmochim. Acta 57 (7), 1505–1519.
Ashley, R.P., Cunningham, C.G., Bostick, N.H., Dean, W.E., Chou, I.M., 1991. Geology and geochemistry of three sedimentary-rock-hosted disseminated gold deposits in Guizhou Province, People's Republic of China. Ore Geol. Rev. 6 (2), 133–151.
Bakken, B.M., Einaudi, M.T., 1986. Spatial and temporal relations between wall rock alteration and gold mineralization, Main pit, Carlin gold mine, Nevada, USA, Gold. pp. 388–403.
Barker, S.L.L., Hickey, K.A., Cline, J.S., Dipple, G.M., Kilburn, M.R., Vaughan, J.R., Longo, A.A., 2009. Uncloaking invisible gold: use of nanosims to evaluate gold, trace elements, and sulfur isotope in pyrite from Carlin-type gold. Econ. Geol. 104 (7), 897–904.
Barker, S.L.L., Dipple, G.M., Hickey, K.A., Lepore, W.A., Vaughan, J.R., 2013. Applying stable isotopes to mineral exploration: teaching an old dog new tricks. Econ. Geol. 108 (1), 1–9.
Bloomstein, E.I., Massingill, G.L., Parratt, R.L., Peltonen, D.R., 1991. Discovery, Geology, and Mineralization of the Rabbit Creek Gold Deposit, Humboldt County, Nevada, Geology and Ore Deposits of the Great Basin: Reno, Geological Society of Nevada, Symposium Proceedings, pp. 821–843.
Bogoch, R., Eldad, H., Yaacov, N., 1984. Scandium-bearing carbonates of the Tarr albitite complex, southeast Sinai. Geochim. Cosmochim. Acta 48 (4), 885–887.
Cail, T.L., Cline, J.S., 2001. Alteration associated with gold deposition at the Getchell Carlin-type gold deposit, north-central Nevada. Econ. Geol. 96 (6), 1343–1359.
Chen, M.H., Mao, J.W., Bierlein, F.P., Norman, T., Uttley, P.J., 2011. Structural features and metallogenesis of the Carlin-type Jinfeng (Lannigou) gold deposit, Guizhou Province, China. Ore Geol. Rev. 43 (1), 217–234.
Chen, M.H., Zhang, Z.Q., Santosh, M., Dang, Y., Zhang, W., 2014. The Carlin-type gold deposits of the "Golden Triangle" of SW China: Pb and S isotopic constraints for the ore genesis. J. Asian Earth Sci. http://dx.doi.org/10.1016/j.jseaes.2014.08.022.
Chen, M.H., Mao, J.W., Li, C., Zhang, Z.Q., Dang, Y., 2015. Re–Os isochron ages for arsenopyrite from Carlin-like gold deposits in the Yunnan–Guizhou–Guangxi "golden triangle", southwestern China. Ore Geol. Rev. 64, 316–327.
Cline, J.S., Hofstra, A.A., 2000. Ore-fluid evolution at the Getchell Carlin-type gold deposit, Nevada, USA. Eur. J. Mineral. 12 (1), 195–212.
Cline, J.S., Hofstra, A.H., Muntean, J.L., Tosdal, R.M., Hickey, K.A., 2005. Carlin-type gold deposits in Nevada: critical geologic characteristics and viable models. Economic Geology 100th Anniversary Volume, pp. 451–484.
Cline, J.S., Muntean, J.L., Gu, X.X., Xia, Y., 2013. A comparison of Carlin-type gold deposits: Guizhou Province, golden triangle, southwest China, and northern Nevada, USA. Earth Sci. Front. 20 (1), 1–18.
Cunningham, C.G., Ashley, R.P., Chou, I.M., Huang, Z.S., Wan, C.Y., Li, W.K., 1988. Newly discovered sedimentary rock-hosted disseminated gold deposits in the People's Republic of China. Econ. Geol. 83 (7), 1462–1467.
de Almeida, C.M., Olivo, G.R., Chouinard, A., Weakly, C., Poirier, G., 2010. Mineral paragenesis, alteration, and geochemistry of the two types of gold ore and the host rocks from the Carlin-type deposits in the southern part of the Goldstrike property, northern Nevada: Implications for sources of ore-forming elements, ore genesis, and mineral exploration. Econ. Geol. 105 (5), 971–1004.
Eby, G.N., 1973. Scandium geochemistry of Oka carbonatite complex, Oka, Quebec. Am. Mineral. 58 (9–10), 819–825.
Emsbo, P., Groves, D.I., Hofstra, A.H., Bierlein, F.P., 2006. The giant Carlin gold province: a protracted interplay of orogenic, basinal, and hydrothermal processes above a lithospheric boundary. Mineral. Deposita 41 (6), 517–525.
Finlowbates, T., Stumpfl, E.F., 1981. The behaviour of so-called immobile elements in hydrothermally altered rocks associated with volcanogenic submarine-exhalative ore deposits. Mineral. Deposita 16 (2), 319–328.
Fortuna, J., Kesler, S.E., Stenger, D.P., 2003. Source of iron for sulfidation and gold deposition, Twin Creeks Carlin-type deposit, Nevada. Econ. Geol. 98 (6), 1213–1224.
Fu, S.H., Gu, X.X., Wang, Q., Xia, Y., Zhang, X.C., Tao, Y., 2004. The typomorphic characteristics of gold-bearing pyrites from Shuiyindong gold deposit, SW Guizhou. Acta Mineral. Sin. 24 (1), 75–80 (in Chinese with English abstract).
Grant, J.A., 1986. The isocon diagram: a simple solution to Gresens' equation for metasomatic alteration. Econ. Geol. 81 (8), 1976–1982.
Gresens, R.L., 1967. Composition–volume relationships of metasomatism. Chem. Geol. 2, 47–65.
Gu, X.X., Li, B.H., Xu, S.H., Fu, S.H., Dong, S.Y., 2007. Characteristics of hydrocarhon-bearing ore-forming fluids in the Youjiang Basin, South China: implication for hydrocarbon accumulation and ore mineralization. Earth Sci. Front. 14 (05), 133–146 (in Chinese with English abstract).
Gu, X.X., Zhang, Y.M., Li, B.H., Dong, S.Y., Xue, C.J., Fu, S.H., 2012. Hydrocarbon- and ore-bearing basinal fluids: a possible link between gold mineralization and hydrocarbon accumulation in the Youjiang basin, South China. Mineral. Deposita 47 (6), 663–682.
Hausen, D.M., 1967. Fine Gold Occurrence at Carlin, Nevada. Columbia University, New York (166 pp.).
He, M.Y., 1996. Physicochemical conditions of differential mineralization of Au and As in gold deposits, southwest Guizhou Province, China. Chin. J. Geochem. 15 (2), 189–192.
Heinrich, C.A., Eadington, P.J., 1986. Thermodynamic predictions of the hydrothermal chemistry of arsenic, and their significance for the paragenetic sequence of some cassiterite–arsenopyrite-base metal sulfide deposits. Econ. Geol. 81 (3), 511–529.
Heitt, D.G., Dunbar, W.W., Thompson, T.B., Jackson, R.G., 2003. Geology and geochemistry of the Deep Star gold deposit, Carlin Trend, Nevada. Econ. Geol. 98 (6), 1107–1135.
Hickey, K.A., Ahmed, A.D., Barker, S.L., Leonardson, R., 2014a. Fault-controlled lateral fluid flow underneath and into a Carlin-type gold deposit: isotopic and geochemical footprints. Econ. Geol. 109 (5), 1431–1460.
Hickey, K.A., Barker, S.L., Dipple, G.M., Arehart, G.B., Donelick, R.A., 2014b. The brevity of hydrothermal fluid flow revealed by thermal halos around giant gold deposits: implications for Carlin-type gold systems. Econ. Geol. 109 (5), 1461–1487.
Hofstra, A.H., 1994. Geology and genesis of the Carlin-type gold deposits in the Jerritt Canyon district, Nevada: Unpublished Ph. D, dissertation, Boulder, University of Colorado.
Hofstra, A.H., Cline, J.S., 2000. Characteristics and models for Carlin-type gold deposits. Rev. Econ. Geol. 13, 163–220.
Hofstra, A.H., Leventhal, J.S., Northrop, H.R., Landis, G.P., Rye, R.O., Birak, D.J., Dahl, A.R., 1991. Genesis of sediment-hosted disseminated-gold deposits by fluid mixing and

sulfidization: chemical-reaction-path modeling of ore-depositional processes documented in the Jerritt Canyon district, Nevada. Geology 19 (1), 36–40.
Hofstra, A.H., John, D.A., Theodore, T.G., 2003. A special issue devoted to gold deposits in northern Nevada: part 2. Carlin-type deposits. Econ. Geol. 98 (6), 1063–1067.
Hofstra, A.H., Emsbo, P., Christiansen, W.D., Theodorakos, P., Zhang, X.C., Hu, R.Z., Su, W.C., Fu, S.H., 2005. Source of Ore Fluids in Carlin-type Gold Deposits, China: Implications for Genetic Models. Springer, pp. 533–536.
Hu, R.Z., Su, W.C., Bi, X.W., Tu, G.Z., Hofstra, A.H., 2002. Geology and geochemistry of Carlin-type gold deposits in China. Mineral. Deposita 37 (3–4), 378–392.
Kesler, S.E., Fortuna, J., Ye, Z.J., Alt, J.C., Core, D.P., Zohar, P., Borhauer, J., Chryssoulis, S.L., 2003. Evaluation of the role of sulfidation in deposition of gold, Screamer section of the Betze–Post Carlin-type deposit, Nevada. Econ. Geol. 98 (6), 1137–1157.
Kesler, S.E., Riciputi, L.C., Ye, Z.J., 2005. Evidence for a magmatic origin for Carlin-type gold deposits: isotopic composition of sulfur in the Betze–Post–Screamer deposit, Nevada, USA. Mineral. Deposita 40 (2), 127–136.
Kuehn, C.A., Rose, A.W., 1992. Geology and geochemistry of wall-rock alteration at the Carlin gold deposit, Nevada. Econ. Geol. 87 (7), 1697–1721.
Kuehn, C.A., Rose, A.W., 1995. Carlin gold deposits, Nevada: origin in a deep zone of mixing between normally pressured and overpressured fluids. Econ. Geol. 90 (1), 17–36.
Li, C.-P., Peters, S.G., 1999. Comparative Geology and Geochemistry of Sedimentary-rock-hosted (Carlin-type) Gold Deposits in the People's Republic of China and in Nevada, USA. (Master's Thesis). University of Nevada, Reno.
Liu, J.Z., 2001. The geology of the yanshang gold deposit, Zhenfeng county, Guizhou. Guizhou Geol. 8 (3), 174–178 (in Chinese with English abstract).
Liu, J.Z., 2003. Ore characteristics and gold occurrence of the Shuiyindong gold deposit, Guizhou. Guizhou Geol. 20 (1), 30–34 (in Chinese with English abstract).
Liu, J.M., Ye, J., Ying, H.L., Liu, J.J., Zheng, M.H., Gu, X.X., 2002. Sediment-hosted microdisseminated gold mineralization constrained by basin paleo-topographic highs in the Youjiang basin, South China. J. Asian Earth Sci. 20 (5), 517–533.
Liu, J.Z., Xia, Y., Deng, Y.M., Su, W.C., Xing Chun, Z., Qiu, L., Chen, M., Chen, F.E., Fu, Z.K., 2009. Researches on the SBT of Shuiyindong gold deposit and significance for regional prospecting. Gold Sci. Technol. 17 (03), 1–5 (in Chinese with English abstract).
Liu, S., Su, W.C., Hu, R.Z., Feng, C.X., Gao, S., Coulson, I.M., Wang, T., Feng, G.Y., Tao, Y., Xia, Y., 2010. Geochronological and geochemical constraints on the petrogenesis of alkaline ultramafic dykes from southwest Guizhou Province, SW China. Lithos 114 (1), 253–264.
Longo, A.A., Cline, J.S., Muntean, J.L., 2009. Using pyrite to track evolving fluid pathways and chemistry in Carlin-type deposits. In: Williams, P.J. (Ed.), 2009 Portland GSA Annual Meeting.
Lubben, J.D., Cline, J.S., Barker, S.L.L., 2012. Ore fluid properties and sources from quartz-associated gold at the Betze–Post Carlin-type gold deposit, Nevada, United States. Econ. Geol. 107 (7), 1351–1385.
Muntean, J.L., Coward, M.P., Tarnocai, C.A., 2007. Reactivated palaeozoic normal faults: controls on the formation of Carlin-type gold deposits in north-central Nevada. Special Publication—Geological Society of London 272, p. 571.
Muntean, J.L., Cassinerio, M.D., Arehart, G.B., Cline, J.S., Longo, A.A., 2010. Fluid pathways at the Turquoise Ridge Carlin-type gold deposit, Getchell district, Nevada. Smart Science for Exploration and Mining vol. 1 and 2 (251–253 pp.).
Muntean, J.L., Cline, J.S., Simon, A.C., Longo, A.A., 2011. Magmatic–hydrothermal origin of Nevada's Carlin-type gold deposits. Nat. Geosci. 4 (2), 122–127.
Peters, S.G., 2004. Syn-deformational features of Carlin-type Au deposits. J. Struct. Geol. 26 (6–7), 1007–1023.
Peters, S.G., Huang, J.Z., Li, Z.P., Cheng Gui, J., 2007. Sedimentary rock-hosted Au deposits of the Dian–Qian–Gui area, Guizhou, and Yunnan Provinces, and Guangxi District, China. Ore Geol. Rev. 31 (1), 170–204.
Radtke, A.S., Scheiner, B.J., 1970. Studies of hydrothermal gold deposition — (pt.) 1, Carlin gold deposit, Nevada, the role of carbonaceous materials in gold deposition. Econ. Geol. 65 (2), 87–102.
Radtke, A.S., Heropoulos, C., Fabbi, B.P., Scheiner, B.J., Essington, M., 1972. Data on major and minor elements in host rocks and ores, Carlin gold deposit, Nevada. Econ. Geol. 67 (7), 975–978.
Radtke, A.S., Rye, R.O., Dickson, F.W., 1980. Geology and stable isotope studies of the Carlin gold deposit, Nevada. Econ. Geol. 75 (5), 641–672.
Rubin, J.N., Henry, C.D., Price, J.G., 1993. The mobility of zirconium and other "immobile" elements during hydrothermal alteration. Chem. Geol. 110 (1–3), 29–47.
Seward, T.M., 1973. Thio complexes of gold and the transport of gold in hydrothermal ore solutions. Geochim. Cosmochim. Acta 37 (3), 379–399.
Seward, T.M., 1984. The transport and deposition of gold in hydrothermal systems. Gold 165–181.
Simon, G., Huang, H., Penner-Hahn, J.E., Kesler, S.E., Kao, L.S., 1999a. Oxidation state of gold and arsenic in gold-bearing arsenian pyrite. Am. Mineral. 84 (7–8), 1071–1079.
Simon, G., Kesler, S.E., Chryssoulis, S., 1999b. Geochemistry and textures of gold-bearing arsenian pyrite, Twin Creeks, Nevada: implications for deposition of gold in Carlin-type deposits. Econ. Geol. 405–421.
Stenger, D.P., Kesler, S.E., Peltonen, D.R., Tapper, C.J., 1998. Deposition of gold in Carlin-type deposits: the role of sulfidation and decarbonation at Twin Creeks, Nevada. Econ. Geol. Bull. Soc. Econ. Geol. 93 (2), 201–215.
Su, W.C., 2002. The hydrothermal fluid geochemistry of the Carlin-type gold deposits in the southwestern Yangtze Craton, China. Unpublished Ph. D Thesis, Institute of Geochemistry, Chinese Academy of Sciences, Guizhou, china (in Chinese with English abstract).
Su, W.C., Xia, B., Zhang, H.T., Zhang, X.C., Hu, R.Z., 2008. Visible gold in arsenian pyrite at the Shuiyindong Carlin-type gold deposit, Guizhou, China: implications for the environment and processes of ore formation. Ore Geol. Rev. 33 (3), 667–679.
Su, W.C., Heinrich, C.A., Pettke, T., Zhang, X.C., Hu, R.Z., Xia, B., 2009a. Sediment-hosted gold deposits in Guizhou, China: products of wall-rock sulfidation by deep crustal fluids. Econ. Geol. 104 (1), 73–93.
Su, W.C., Hu, R.Z., Xia, B., Xia, Y., Liu, Y.P., 2009b. Calcite Sm–Nd isochron age of the Shuiyindong Carlin-type gold deposit, Guizhou, China. Chem. Geol. 258 (3), 269–274.
Su, W.C., Zhang, H.T., Hu, R.Z., Ge, X., Xia, B., Chen, Y.Y., Zhu, C., 2012. Mineralogy and geochemistry of gold-bearing arsenian pyrite from the Shuiyindong Carlin-type gold deposit, Guizhou, China: implications for gold depositional processes. Mineral. Deposita 47 (6), 653–662.
Theodore, T.G., Kotlyar, B.B., Singer, D.A., Berger, V.I., Abbott, E.W., Foster, A.L., 2003. Applied geochemistry, geology, and mineralogy of the northernmost Carlin Trend, Nevada. Econ. Geol. 98 (2), 287–316.
Vaughan, J.R., Hickey, K., Barker, S., Dipple, G.M., 2010. Stable isotopes and fluid flow pathways in the Banshee Carlin-type gold deposit. Smart Science for Exploration and Mining vol. 1 and 2 (266–268 pp.).
Wang, Z.P., Xia, Y., Song, X.Y., Liu, J.Z., Yang, C.F., Yan, B.W., 2013. Study on the evolution of ore-formation fluids for Au–Sb ore deposits and the mechanism of Au–Sb paragenesis and differentiation in the southwestern part of Guizhou Province, China. Chin. J. Geochem. 32 (1), 56–68.
Williams-Jones, A.E., Norman, C., 1997. Controls of mineral parageneses in the system Fe–Sb–SO. Econ. Geol. 92 (3), 308–324.
Wood, S.A., Samson, I.M., 2006. The aqueous geochemistry of gallium, germanium, indium and scandium. Ore Geol. Rev. 28 (1), 57–102.
Xia, Y., 2005. Characteristics and model for Shuiyindong gold deposit in southwestern Guizhou, China. Unpublished Ph. D Thesis, Institute of Geochemistry, Chinese Academy of Sciences, Guizhou, China (in Chinese with English abstract).
Ye, Z.J., Kesler, S.E., Essene, E.J., Zohar, P.B., Borhauer, J.L., 2003. Relation of Carlin-type gold mineralization to lithology, structure and alteration: Screamer zone, Betze–Post deposit, Nevada. Mineral. Deposita 38 (1), 22–38.
Yigit, O., Hofstra, A.H., 2003. Lithogeochemistry of Carlin-type gold mineralization in the Gold Bar district, Battle Mountain–Eureka Trend, Nevada. Ore Geol. Rev. 22 (3–4), 201–224.
Zhang, X.C., Spiro, B., Halls, C., Stanley, C.J., Yang, K.Y., 2003. Sediment-hosted disseminated gold deposits in Southwest Guizhou, PRC: their geological setting and origin in relation to mineralogical, fluid inclusion, and stable-isotope characteristics. Int. Geol. Rev. 45 (5), 407–470.
Zhang, H.T., Su, W.C., Tian, J.J., Liu, Y.P., Liu, J.Z., Liu, C.Q., 2008. Occurrence of gold in the Shuiyingdong Carlin-type gold deposit, Guizhou. Acta Mineral. Sin. 28 (1), 17–24 (in Chinese with English abstract).
Zhang, Y., Xia, Y., Su, W.C., Tao, Y., Zhang, X.C., Liu, J.Z., Deng, Y.M., 2010. Metallogenic model and prognosis of the Shuiyindong super-large strata-bound Carlin-type gold deposit, southwestern Guizhou Province, China. Chin. J. Geochem. 29 (2), 157–166.
Zhuang, H.P., Lu, J.L., Fu, J.M., Ren, C.G., Zou, D.G., 1999. Crude oil as carrier of gold: Petrological and geochemical evidence from Lannigou gold deposit in southwestern Guizhou, China. Sci. China Ser. D Earth Sci. 42 (2), 216–224.